

# Mineralogical and geochemical characterization of high-medieval lead–silver smelting slags from Wiesloch near Heidelberg (Germany)—an approach to process reconstruction

Florian Ströbele · Thomas Wenzel · Andreas Kronz · Ludwig H. Hildebrandt · Gregor Markl

Received: 18 November 2009 / Accepted: 26 May 2010 / Published online: 30 July 2010  
© Springer-Verlag 2010

**Abstract** Here, we present detailed electron microprobe analyses and age data of high-medieval lead–silver smelting slags. The mineral composition data provide a database of all silicate and oxide phases in the slag. Bulk chemistry as well as mineral composition is used to reconstruct liquidus, solidus, and viscosity of the slag melt. By calculating the mass balance of the smelting process, a mass ratio of the various compounds used in the smelting process is determined. Through this we were able to discriminate qualitatively between non-ferrous metal smelting slags and bloomery slags. We also report a new type and process of silver production in which argentiferous galmei (zinc carbonate) was used as a main silver ore together with galena. The results indicate a sophisticated high-medieval smelting technology, in which a slag with a low liquidus and a low viscosity was created.

**Keywords** Lead–silver smelting slags · Smelting process · Mineralogical and geochemical characterization

## Introduction

The area of Wiesloch near Heidelberg (SW-Germany) has seen mining activities for at least 2,000 years as the oxidation zone of the carbonate-hosted lead–zinc deposit of the so-called Mississippi Valley-Type (MVT, Hildebrandt 1997, 1998, 2004; Pfaff et al. 2010) was exploited for lead and silver ores since Roman times (Hildebrandt 2004). The smelting activities resulted in large slag dumps of ~400,000 t of which 360,000 t result from smelting of argentiferous galmei and galena, from the late tenth to the late twelfth century (Hildebrandt 1997, 1998). For better understanding, a list of minerals and their chemical formulae, which are used in this paper, is given in Table 1.

Although the workflow of the historic lead/silver smelting process is known quite well (a good overview is given by Goldenberg et al. 1996), there is still a gap of knowledge concerning the composition of the furnace charge. In Wiesloch, no furnace remains have been found yet. Metals related directly to the smelting process and not to the casting of artifacts are very rare. Despite this fact, detailed slag analyses can be used to gain knowledge on the smelting process and its specific conditions.

Many papers have been published on ancient iron-smelting slags (e.g., Eggers 1999; Kronz and Eggers 2001; Kronz and Keesmann 2003; Kronz 2005; Bauermeister 2005; Bauermeister and Kronz 2006), while there are only few studies on slags of non-ferrous metal production, specifically about those of lead smelting (Bachmann

---

F. Ströbele (✉) · T. Wenzel · G. Markl  
Institut für Geowissenschaften,  
Eberhard Karls Universität Tübingen,  
Wilhelmstraße 56,  
72074 Tübingen, Germany  
e-mail: markl@uni-tuebingn.de

A. Kronz  
Geowissenschaftliches Zentrum,  
Georg August Universität Göttingen,  
Goldschmidt Strasse 1,  
37077 Göttingen, Germany

L. H. Hildebrandt  
Büro für Denkmalpflege und Umweltschutz,  
Im Köpfle 7,  
69168 Wiesloch, Germany

**Table 1** Formulae of minerals

Olivine	Fayalite	$\text{Fe}_2\text{SiO}_4$
	Forsterite	$\text{Mg}_2\text{SiO}_4$
	Larnite	$\text{Ca}_2\text{SiO}_4$
	Tephroite	$\text{Mn}_2\text{SiO}_4$
	Monticellite	$\text{CaMgSiO}_4$
	Kirschsteinite (Zn-olivine)	$\text{CaFeSiO}_4$ $\text{Zn}_2\text{SiO}_4$
Spinel	Magnetite	$\text{Fe}^{2+}\text{Fe}_2^{3+}\text{O}_4$
	Gahnite	$\text{ZnAl}_2\text{O}_4$
	Ulvöspine	$\text{Fe}_2^{2+}\text{TiO}_4$
	Hercynite	$\text{FeAl}_2\text{O}_4$
	Spinel s.s.	$\text{MgAl}_2\text{O}_4$
	Galaxite	$(\text{Mn,Fe,Mg})(\text{Al,Fe})_2\text{O}_4$
	Other slag minerals	Leucite
Hyalophane		$(\text{K,Ba})[\text{Al}(\text{Si,Al})\text{Si}_2\text{O}_8]$
Iscoreite		$\text{Fe}_2^{3+}\text{Fe}_5^{2+}\text{SiO}_{10}$
Wüstite		$\text{Fe}_x\text{O}$
Hedenbergite		$\text{CaFeSi}_2\text{O}_6$
Speiss phases	Unnamed phase	$\text{Fe}_2\text{As}$
	Westerveldite	$(\text{Fe,Ni,Co})\text{As}$
	Löllingite	$\text{FeAs}_2$
	Troilite	$\text{FeS}$
Other phases	Rhönite	$\text{Ca}_2(\text{Mg,Fe}^{2+}\text{Fe}^{3+}\text{Ti})_6[\text{O}_2(\text{Si,Al})_6\text{O}_{18}]$
	Melilite	$(\text{Ca,Na})_2(\text{Al,Mg,Fe}^{2+})[(\text{Al,Si})\text{SiO}_7]$
	Litharge	$\text{PbO}$
Ores	Galena	$\text{PbS}$
	Sphalerite	$\text{ZnS}$
	Hydrozincite	$\text{Zn}_5[(\text{OH})_3 \text{CO}_3]_2$
	Smithsonite	$\text{ZnCO}_3$
	Jordanite	$\text{Pb}_{14}(\text{As,Sb})_6\text{S}_{23}$
	Geocronite	$\text{Pb}_{14}(\text{Sb,As})_6\text{S}_{23}$
	Fluxes	Calcite
Dolomite		$\text{CaMg}(\text{CO}_3)_2$
Baryte		$\text{BaSO}_4$
Quartz		$\text{SiO}_2$
Hematite		$\text{Fe}_2\text{O}_3$
Goethite		$\alpha\text{-FeO}(\text{OH})$

1993b; Hauptmann et al. 1988; Pernicka 1981, 1983; Pernicka et al. 1985). The first detailed publication on the mineralogical analysis of lead smelting slags (Faber 1936) gives an overview on slag mineralogy and chemistry but is mainly descriptive. More recent publications focus on ancient slags from the Cyclades, predominantly, where galena was smelted, no fluxes were used, and the smelting was done only to produce silver but not lead (Pernicka et

al. 1985). Other publications like Battle and Hager (1990), Degterov and Pelton (1999), Ettler et al. (2001), Kongoli and Yazawa (2001), Muszer (2006), Nikolic et al. (2008a, b) and Schlesinger and Lynch (1986) focus on smelting slags dating from the nineteenth and twentieth century. Due to the differences in the age of the slags and the differences in the smelting processes, it is difficult to compare the published results to our observations from Wiesloch.

Studies on the slags of Wiesloch have been published by Hildebrandt (1997, 1998). A further study by Kappes (2000) deals with soil contaminations from the slag heap but does not give bulk composition analyses of slag material. This study also reports that the smelting process is ineffective due to the high zinc content which will be discussed later.

It is the aim of the present contribution to interpret in detail the slags of the historic mining area around Wiesloch and to reconstruct the process of their formation as an example of medieval silver smelting technology based on unusually Zn-rich ores. Our reconstruction of the historical smelting process includes process temperatures, properties of the slag, ratio of fluxes, and fuel as well as the technology, e.g., the type of furnace. It is based on mineralogical, petrological, and geochemical analyses of Wiesloch slags to determine the chemical properties of the slag and the physical characteristics of the slag melt.

#### Geological and historical background

The MVT deposit of Wiesloch (Hildebrandt 1997, 1998; Pfaff et al. 2010) is related to the extensional tectonic setting of the Upper Rhinegraben. The mineralized area can be found between the Rhinegraben main fault (W) and the villages of Leimen (N), Mauer (NE), Sinsheim (E) and Bruchsal (S). The mineralization is concentrated in the carbonates of the Middle Triassic, namely the Trochitenkalk (mo1) and the Schaumkalk (mu2s). The mineralization consists predominantly of crystalline sphalerite and a second variety of sphalerite (Schalenblende), which is amorphous and banded (also called colloform), galena and pyrite (Seeliger 1963; Hildebrandt 1997, 1998; Pfaff et al. 2010).

Mining activities have been verified at least since the Roman times (Mone 1859). The most intense historic mining activities took place between 950 and 1080 (Hildebrandt 1997, 1998). Since then, no mine trying to exploit galena or galmei profitably survived longer than 30 years. The deposit experienced a last boom between 1845 and 1880, when thousands of tons of galmei backfill were found in high-medieval or even Roman galleries. The exploitation of the deposit lasted until 1954, when the last mining facilities were abandoned. For a detailed description of all mining periods, see Hildebrandt (1997, 1998, 2004, 2005).

## Sample material

Because of the anthropogenic influence and weathering conditions, sampling campaigns in slag heaps need some extra care: Samples for the determination of the bulk composition should not contain several pieces of slag to avoid mixing analyses of slags which result from different processes or which were brought to the dump later. All bulk analyses listed below refer to one single piece of slag. Slag samples derive from the construction pit of the “Palatin Congress Centre” (built 1992, the spoil dump known as *Schafbuckelhalde* was sampled (Fig. 1)). Stratified samples from slag dumps of the surrounding villages came from collections. To be able to sample the slag heap in situ, a pit with a depth of 3.5 m on the plots 156 and 157 (Amalienstraße, D-69168 Wiesloch) was excavated. All samples are in situ and were taken from the wall of the pit.

It will be shown later that galmei is an important ore in Wiesloch. Galmei is a weathering product of sphalerite and is also called calamine. It is composed mainly of smithsonite, but also some Zn carbonates (hydrozincite and hemimorphite) can occur. The fraction of a mineral in this mixture is variable. This is why no mineral name but the term galmei will be used in this paper.

## Analytical and experimental methods

### Accelerated mass spectrometry dating of sample material

Three samples from different depths (15S1, 1 m; 15S3, 1.3 m; 15S8, 2.8 m) of the excavation pit were dated using the  $^{14}\text{C}$ -method. Additionally, one sample from the *Schafbuckelhalde* was dated. To avoid contamination with

modern organic carbon, only charcoal pieces that were embedded completely in the slag were picked for accelerated mass spectrometry (AMS) dating. The sample processing was performed at the radiocarbon laboratory at Heidelberg by Dr. Kromer. The analyses were conducted at the radiocarbon laboratory of the Department of Physics at Lund University (Sweden) according to the procedure described in Skog (2007).

### Determination of the wood species

It is important for the reconstruction of the smelting process to know the type of wood used for the production of the charcoal. To get information on the charcoal ash composition, several inclusions of charcoal were picked from the slag and analysed at a dendrochronological laboratory in Hemmenhofen, Germany, for determination of the wood species by microscopic analysis of oriented sections.

### Production of the quenched beads

Bulk analyses of slags are often difficult because of liquid immiscibility phenomena and partially molten inclusions. Here, we tried to estimate the bulk composition of the silicate fraction of our slag, which was usually between ~85 and ~99 wt.%. For this purpose, samples were ground in a cross beater mill. Visible speiss inclusions were removed by handpicking; the remaining material was homogenized in an agate mortar. Usually, bulk chemistry of slags is done by XRF. Since our sample material can contain small but significant amounts of As (in form of extremely small speiss inclusions, which could not be removed by handpicking), which would react or form alloys with Pt crucibles, standard XRF preparation could not be applied.

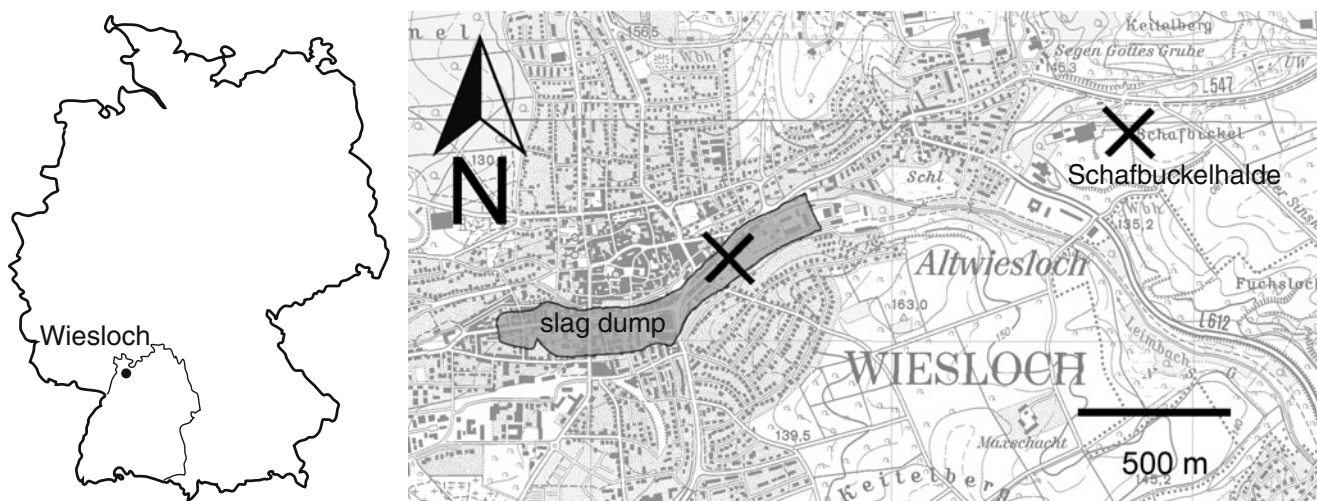


**Fig. 1** Map of Wiesloch, showing the dimensions of the high-medieval slag dump (gray field, after Hildebrandt 1998) and sampling localities. The cross in the right shows the location of

the *Schafbuckelhalde*. As base for the map, the TK-25 data from the Landesvermessungsamt Baden-Württemberg were used

Another reason not to use XRF is the composition of XRF basalt standards, which have a maximum of ~10% FeO (in contrary to the slags with up to 50%). Therefore, the XRF-standards are not appropriate for slags. Of the sample powder, 30 mg was charged with water on a Pt wire and molten at 1,300°C in a vertically mounted graphite tube resistance furnace (former AAS) within an Ar atmosphere. The molten samples were quenched in water, mounted in epoxy resin and polished for electron microprobe (EMP) analysis. All heating steps as well as the release of the sample into a quenching flask were controlled by a Perkin Elmer AAS control unit (type HGA 400).

While being melted, the samples were observed through a hole in the furnace (diameter 3 mm). Temperature was monitored by the control unit. The melting experiments were conducted at the Geowissenschaftliches Zentrum at the Universität Göttingen, Germany (see details in Kronz (1994, 1997)). Two batches of melting experiments were conducted. The first batch (B1) provided data for the estimation of solidus and liquidus temperatures of the slags. During melting, some elements evaporated and formed a yellowish, strongly smelling precipitate on the furnace's wall. A qualitative XRF scan showed that the precipitate was composed mainly of Zn, As (originating from micro-inclusions of speiss), and small amounts of S and Fe. To overcome the problem of evaporation, a mixture of 20–25 wt.% Merck Spectromelt A (66 wt.% lithium tetraborate, 34 wt.% lithium metaborate) and sample material was molten at a lower temperature of 1,000°C in a second batch (B2). No evaporation was observed in this run.

#### EMP analysis

Mineral and bulk slag composition was analysed using a JEOL JXA 8900 RL EMP in wavelength dispersive mode at the Institut für Geowissenschaften, Universität Tübingen (Germany). For calibration, natural as well as synthetic standards were used. Silicates and oxides were analysed using an acceleration voltage of 15 kV and a probe current of 20 nA. Bulk samples, glass, sulfides, and arsenides were analysed with 20 kV and 20 nA. Glasses, quenched beads, and leucite were analysed with a defocused beam of 5–20 µm diameter to avoid Na-migration. Counting time on the peak was 16 s for major elements and 30 s for minor elements. The background counting time was always half of the peak counting time. Data reduction was performed using the internal  $\phi\rho Z$  procedures of JEOL (Armstrong 1991). We summarized the detection limits in Table 2.

A peak overlap correction was performed for the hyalophane measurements (Al L $\alpha$  was affected by Ba L $\beta$ ) and for the arsenides (Sb L $\alpha$  was affected by Bi L $\beta$ ; As L $\alpha$  was affected by Sb L $\beta$ ). Calculation of Fe<sup>3+</sup> was conducted following the procedure given by Droop (1987).

**Table 2** Detection limits for EMPA

Oxide	Hyalophane SD (%)	Hyalophane DL (ppm)	Leucite SD (%)	Leucite DL (ppm)	Olivine SD (%)	Olivine DL (ppm)	Iscorite SD (%)	Iscorite DL (ppm)	Spinel SD (%)	Spinel DL (ppm)	Element	Wüstite SD (%)	Wüstite DL (ppm)
SiO <sub>2</sub>	0.55	180	0.43	141	0.37	113	0.68	116	1.45	115	Si	3.39	60
FeO	–	–	–	–	0.55	232	0.62	249	0.49	190	Fe	0.35	194
Fe <sub>2</sub> O <sub>3</sub>	1.5	374	3.23	232	–	–	–	–	–	–	Mg	6.2	40
MgO	–	–	–	–	2.07	80	2.72	71	2.39	69	Al	3.13	40
MnO	–	–	–	–	6.87	161	3.4	181	4.9	130	Ti	4.53	85
CaO	7.7	217	7.36	171	2.66	92	6.88	111	12.4	107	Zn	1.38	557
ZnO	–	–	–	–	1.74	315	1.59	374	1.32	520	Mn	7.63	148
Na <sub>2</sub> O	58.11	327	6.29	254	27.98	96	–	–	–	–	Ca	6.58	99
K <sub>2</sub> O	2.53	200	1.01	167	–	–	–	–	–	–	O	0.25	145
BaO	1.09	654	3.15	393	–	–	–	–	–	–			
Al <sub>2</sub> O <sub>3</sub>	0.8	203	0.69	168	21.14	69	1.32	79	0.39	79			
TiO <sub>2</sub>	4.42	271	15.77	171	–	–	2.59	112	1.34	111			
P <sub>2</sub> O <sub>5</sub>	38.6	243	46.12	176	–	–	–	–	–	–			



Bloomery experiment

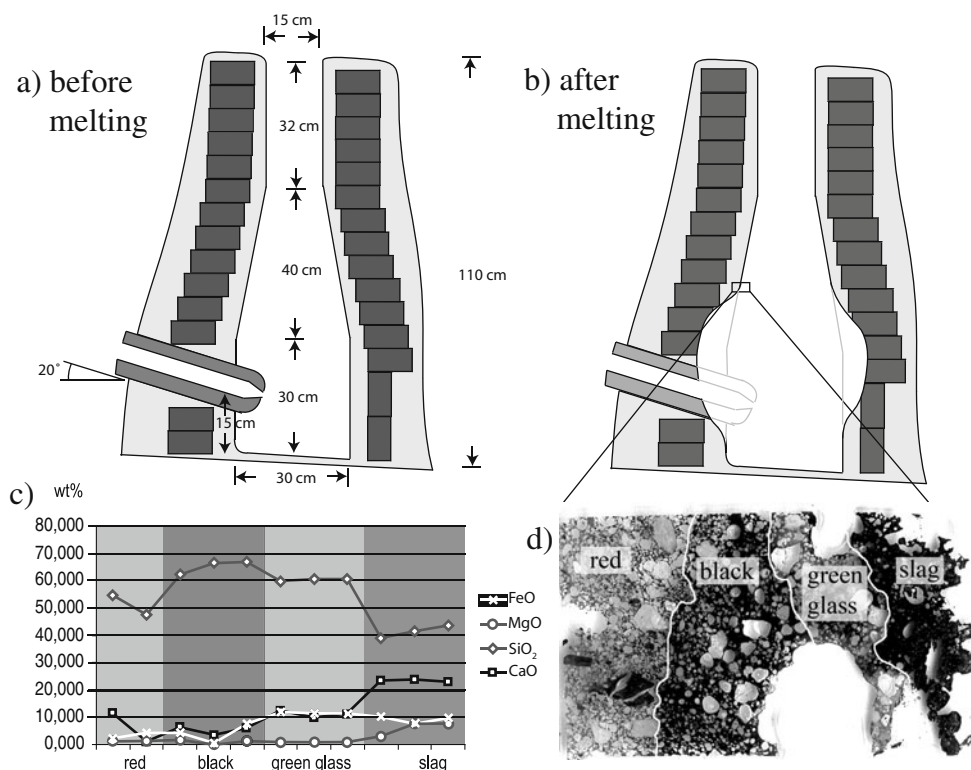
It will be shown later that an important factor in the process of reconstruction is the fraction of furnace lining in the slag and the type of interaction between slag melt and furnace lining. The type of interaction of the slag melt and the refractories of the furnace wall is not well known yet. Possible processes are assimilation, eutectic melting, or dissolution. All these have a different influence on the final slag chemistry. Although a description of the resulting textures can be found in Craddock et al. (1985), information on “metasomatic” processes is still absent. In order to gain more information, a bloomery experiment was conducted in summer 2009. Although the slags from bloomery differ from the ones of non-ferrous-metal smelting, the bloomery process was chosen because it was easier to conduct, and there was no danger of lead contamination of the soil underneath the furnace. The exact dimensions of the furnace were defined by a wooden form. Three tuyères were inserted in a 120° geometry. Each tuyère was inclined against the center of the furnace by 20° (Fig. 2). The tuyères were connected to double-acting bellows to ensure continuous air supply. The wall of the furnace was made of ordinary bricks to support the structure. The lining and the rendering of the furnace, as well as the tuyères, were made of clay (grogged with quartz sand). The furnace was fired with a wood fire for drying

and was allowed to cool down after the drying process to be able to sample the furnace lining before smelting. To produce slags, which are as close as possible to the Wiesloch slag composition, a charge of 200 g bean ore and 15 g calcite was calculated using the mass balances given by Kronz and Keesmann (2003). The calcite was added to reach a CaO content of the slag of ~7–10 wt.%, as observed in the Wiesloch slag (Table 9). The chemistry of the resulting bloomery slag should be close to the Wiesloch slag and thus have a similar effect on the furnace lining.

The clay used for the furnace lining and the tuyères was taken from a local quarry in Tübingen, S-Germany (Nagel quarry, Pfrondorf) and originates from the lower parts of Lias α (Lower Jurassic). The ore was taken from a Malm (Upper Jurassic) karst cave (Sonnenbühl/Mössingen, S-Germany), washed through a 3.3-mm sieve, and dried. Carbonates, plants, and other impurities were removed by handpicking, before crushing to a size <1 cm. Malm limestone was used as flux.

The charge was composed of alternate layers of charcoal and an ore–calcite mixture in a mass ratio of 2:1. The temperature in front of the tuyères was controlled by an optical pyrometer ( $\epsilon=0.95$ ) and by a Ni/CrNi-thermocouple. Throughout the whole process, the temperature was held at ~1,100°C in front of the tuyères with a short time extreme value of 1,290°C.

**Fig. 2** Design drawing (to scale) of the bloomery furnace before (a) and after smelting (b). Also shown are the picture of a cross section (d) of the furnace lining and its chemical variability (e)



## Results

### AMS dating

The ages of the samples as determined by AMS overlapped between 1051 and 1153 AD within the  $1\sigma$  error of the calibrated ages (calibration: Reimer et al. 2004). Hence, we are sure to deal with high-medieval slags (Table 3).

### Wood used for the charcoal

Most of the picked charcoal inclusions were too small for a clear determination, but gave strong evidence to be either from oak or chestnut. One clearly determined piece was oak. The type of wood used for the production of the charcoal is crucial as it is often the only phase which brings considerable amounts of K into the system, and charcoal from different wood species contains different amounts of K (Matthes 1997).

### Macroscopic texture

Five types of slag can be distinguished macroscopically: M1, a dense, glassy type of a characteristic blue or blue-green colour with a clear fluidal structure; M2, a rare, dense, glassy type of a black colour; M3, a dense microcrystalline or crystalline tap-slag with the typical rope-like structure (below called ropes or rope structure). These ropes show, in most cases, a clear mineralogical stratification. This slag can sporadically contain vugs. Type M4 is dense and (micro)-crystalline without internal macroscopic structures. M5 is a vuggy, (micro)-crystalline type. All of these types show an irregularly shaped, spongy bottom. The shape of the bottom depends on the nature of the hearth or the ground on which the slag solidified. Types M2–M5 occur everywhere in and around Wiesloch, while type M1 was only found in Frauenweiler, a village about 1 km SW of Wiesloch. M3, M4, and M5 are holocrystalline, M1 and M2 contain glass.

### Mineralogical composition

The main mineral in the slags from Wiesloch is olivine, namely fayalite or kirschsteinite. Wüstite and spinel group minerals are very common, while iscorite is typically, but not always present. Leucite occurs rarely. Nearly all

samples contain small speiss drops, which are composed mainly of  $\text{Fe}_2\text{As}$  and troilite, westerveldite and löllingite are very rare. Larger amounts of speiss are often found together with metallic Pb and Sb. Only two samples contain large amounts of hyalophane. One glassy sample contains small crystals of hedenbergite.

### Microscopic structure

Four structural types of slag can be discriminated:

S1, which can only be found in M1, is a glassy type with clear fluidal structure (Fig. 3) and only very few crystals. These crystals are too small for EMPA but were determined by micro X-ray diffraction as hedenbergites. They may form during devitrification, or they nucleate around micro-particles in the melt. S2 contains only wüstite in a glassy to cryptocrystalline matrix. Occasionally, this matrix bears small skeletal olivines. These olivines are too small to be recognized in a microscope; thus, they can only be seen in secondary electron (SE) images in the EMP. This type of slag occurs in morphology types M2 to M5, with predominance in M4 and M5. S3 is crystalline, rope-textured and clearly stratified (Fig. 4). Every rope of the slag shows a mineral stratification which is approximately perpendicular to the surface of the rope. Most of the rope is formed by an inner zone, which is dominated by large, spinifex-textured olivines. This zone changes to an iscorite-dominated zone in which the olivines can disappear completely. The matrix becomes more fine-grained towards the rim of the rope. The outermost rim consists only of a cryptocrystalline to glassy matrix and wüstite. The development of this pattern depends strongly on the size of the rope and is sometimes incomplete or modified. The type of slag can either be dense or vuggy. This texture can be found predominantly in M3, but also in M5. S4 is crystalline, with randomly oriented spinifex olivines. Single minerals such as iscorite occasionally form clusters, but usually the mineral distribution is more or less uniform (Fig. 5). A fining of the grains towards the rims is usually observed. This structure is typical for M4 and M5 slags but can also be seen in M3 (as inner part of the S3). Except for the glassy slag from Frauenweiler, there is no evidence that the mineral content of a slag is related to a certain structure or texture.

**Table 3** AMS results of charcoal from the Wiesloch slags

Sample	Sampling depth (m)	$^{14}\text{C}$ age BP (a)	Cal. ages $1\sigma$	Cal. ages $2\sigma$
Wiesloch 15-1	1	980±50	cal AD 1014–1153	cal AD 973–1180
Wiesloch 15-3	1.3	888±35	cal AD 1051–1210	cal AD 1040–1218
Wiesloch 15-8	2.8	1,010±36	cal AD 986–1115	cal AD 903–1153
Wiesloch 15-P	N/A	893±35	cal AD 1049–1208	cal AD 1039–1216

All samples named 15S\* are from the excavation on the plots 156 and 157, sample 15P is from the *Schafbuckelhalde* (calibration: Reimer et al. 2004)

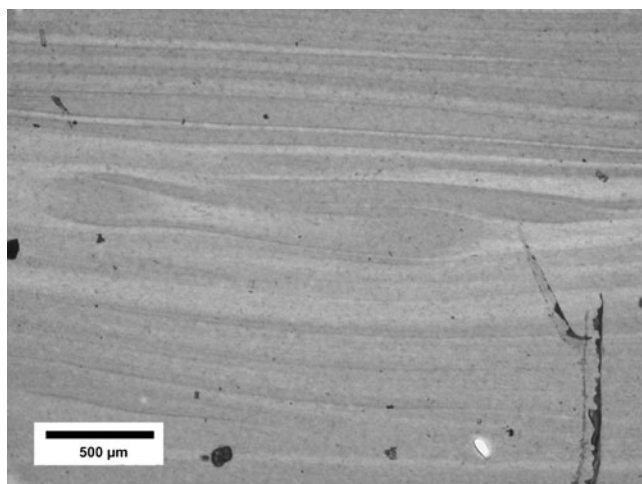


**Fig. 3** Microphoto of microscopic structure S1 in transmitted light showing the fluidal texture

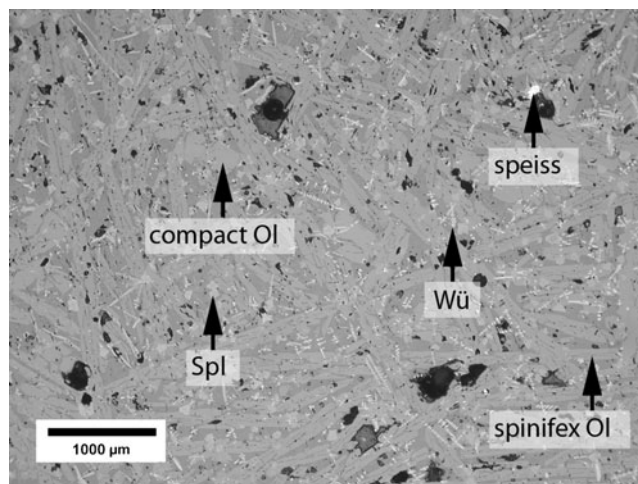


**Fig. 5** Reflected light microphotograph of a slag with homogeneous mineral distribution (S4)

Crystallization sequence

Crystallization sequences are variable in the slags from Wiesloch. It can be linked to the morphology mentioned above (see “[Mineralogical Composition](#)” section):

- M1 Wüstite (±olivine)
- M2 Hedenbergite nucleation or devitrification
- M3 ±Wüstite I → spinel → olivine + spinel → iscorite (±spinel) → wüstite II ± leucite
- M3 (Ba-rich) Wüstite → hyalophane.
- M4 and M5 Spinel → spinel + olivine → iscorite → leucite ± wüstite.

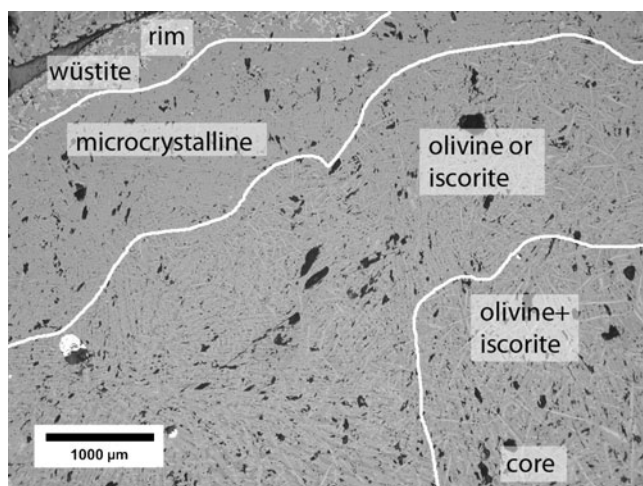


**Fig. 4** Mineral stratification in S3 from a fayalite-dominated zone (*lower right corner*) over a fayalite/iscorite-dominated and a glass-dominated or microcrystalline zone to a wüstite-dominated zone (*upper left corner*). Microphotograph in reflected light

Mineral habit and mineral chemistry

*Olivine*

The most conspicuous feature is the spinifex texture. The crystals are usually a few hundred micrometers long but may reach up to several millimeters in length. In some samples where olivine overgrows spinel, an oriented intergrowth of olivine and spinel was not observed. A second type of olivine crystals is compact and not associated with spinels, but their composition is identical to the spinifex-textured olivines.

Olivine chemistry is quite complex in our system (Table 4). Olivines can be described as a mixture of fayalite, larnite, forsterite, and Zn-olivine (Fig. 6), which is chemically—but not structurally—identical to willemite. A tephroite component is present, but negligible. It proved impossible to analyse profiles in spinifex-textured olivines due to their extreme thinness. Line scans in compact olivines showed a very slight zoning, which cannot be seen in transmitted or reflected light, and also not in SE or BSE images. The cores of the crystals are slightly enriched in forsterite, while the rims are enriched in larnite (Fig. 7a, b). In one sample (15E, type M2/S2), we found a complete mixing series between fayalite and kirschsteinite. Mukhopadhyay and Lindsley (1983) report that the solid solution of fayalite and kirschsteinite is stable above 1,040°C, which indicates the slag was cooled down rapidly after the olivines formed and an exsolution was kinetically inhibited.

Willemite is not present in our samples. A solubility of Zn in olivine and immiscibility between olivine and willemite was assumed previously (Faber 1936) and later shown in experiments (Sarver and Hummel 1962; Ericsson and Filippidis 1986; Jianping et al. 1999). According to these authors, olivine can contain up to 18 mol.% Zn<sub>2</sub>SiO<sub>4</sub>

**Table 4** Representative EPM analyses of olivine including endmember calculations

Sample	15C3_1	15C3_8	15C3_17	15C3_18	15d3_4	15d3_7	15d3_11	15d3_17	15A3_5	15A3_8	15A3_13	15A3_20	15E_5	15E_8	15E_13	15G_1	15G_13
wt.% oxides																	
SiO <sub>2</sub>	30.2	29.2	30.4	30.2	32.9	34.2	33.9	34.1	32.0	32.6	32.1	32.4	30.4	31.0	34.3	33.2	32.6
FeO	61.2	59.4	60.4	61.0	38.8	41.8	42.9	41.2	40.6	38.7	38.5	36.3	47.9	45.3	32.1	34.9	37.2
MgO	1.07	1.62	2.32	2.22	7.29	18.16	12.25	15.04	4.24	3.05	4.49	6.02	1.54	2.24	1.15	5.75	6.48
MnO	0.34	0.34	0.38	0.36	0.39	0.46	0.50	0.48	1.97	1.89	1.97	2.07	0.82	0.98	0.66	1.95	2.06
CaO	1.1	0.9	0.8	0.9	15.7	3.2	5.1	4.5	15.9	18.8	17.3	18.5	10.5	13.7	17.0	20.7	17.6
ZnO	6.1	7.5	5.5	5.6	3.6	2.9	3.4	2.8	5.1	4.8	5.0	4.3	7.3	6.1	7.2	3.5	3.6
Na <sub>2</sub> O	0.08	0.16	0.07	0.14	0.12	0.05	0.09	0.06	0.13	0.07	0.10	0.10	0.24	0.12	0.40	0.08	0.09
Al <sub>2</sub> O <sub>3</sub>	0.12	0.31	0.25	0.34	0.32	0.20	1.62	1.22	0.07	0.11	0.09	0.22	1.21	0.21	4.82	0.10	0.10
total	100.3	99.5	100.2	100.7	99.1	101.0	99.8	99.4	100.0	100.0	99.7	99.9	99.9	99.6	97.6	100.2	99.8
mol.% endmembers																	
Fayalite	87.1	84.4	85.3	85.4	51.3	51.5	57.4	53.7	54.1	52.1	51.3	47.3	67.0	61.9	50.9	45.4	48.6
Forsterite	2.7	4.1	5.8	5.5	17.2	39.8	29.2	34.9	10.1	7.3	10.6	14.0	3.8	5.5	3.3	13.4	15.1
Tephroite	0.5	0.5	0.5	0.5	0.5	0.6	0.7	0.6	2.7	2.6	2.7	2.7	1.2	1.4	1.1	2.6	2.7
Larnite	2.0	1.7	1.5	1.6	26.7	5.0	8.7	7.5	27.1	32.3	29.5	31.0	18.9	23.9	34.6	34.6	29.5
Zn <sub>2</sub> SiO <sub>4</sub>	7.7	9.3	6.8	6.9	4.2	3.1	4.0	3.2	6.0	5.7	5.9	4.9	9.1	7.3	10.1	4.0	4.1
Sum	100.0	100.0	100.0	100.0	100.0	100.0	100.0	100.0	100.0	100.0	100.0	100.0	100.0	100.0	100.0	100.0	100.0

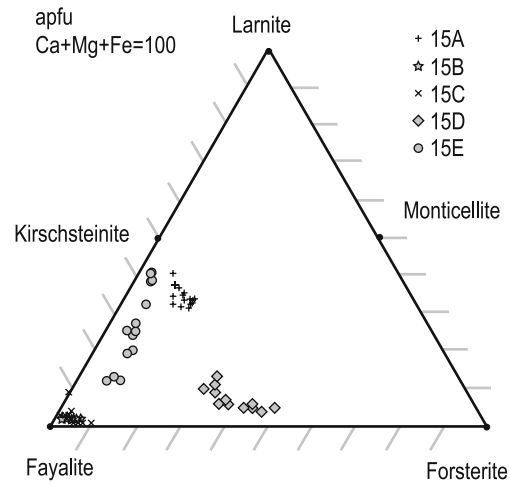


**Fig. 6** Olivine composition in the system fayalite–forsterite–larnite. All samples are from the *Schafbuckelhalde*

at ~1,000°C. This limit is not reached in the Wiesloch slags, the highest Zn<sub>2</sub>SiO<sub>4</sub> content recorded is 10.2 mol.%.

*Spinel*

Spinel forms euhedral crystals, which usually show a strong optical zoning which can be a sector zoning or a growth zoning (Fig. 8). In most samples, spinel is the first phase to crystallize and can be the nucleus for iscorite or wüstite dendrites. It can also be overgrown by olivine, which often inhibits the development of the zoning.

The spinels are not perfectly stoichiometric (Table 5). In addition to elements typical of spinel group minerals, the Wiesloch spinels bear small amounts of Si and Ca. The main endmembers are gahnite and magnetite. In the Fe<sup>2+</sup>–Fe<sup>3+</sup>–Al–Zn diagram (Fig. 9), the spinels show a clear mixing line from gahnite (cores) to magnetite (rims).

*Iscorite*

Fe<sub>2</sub><sup>3+</sup>Fe<sub>5</sub><sup>2+</sup>SiO<sub>10</sub>, also termed as iscorite, is a phase which is not known from natural systems. The phase was first described by Smuts et al. (1968) in material from a reheating furnace of the Pretoria Works of the South African Iron and Steel Industrial Corporation (ISCOR). Smuts et al. (1968) described iscorite as irregularly shaped units or interstitial phase between fayalite and hematite. To our knowledge, iscorite is only found as long laths or needles in historic slags (Fig. 10). Iscorite forms by a reaction of wüstite with fayalite (Smuts 1992) under the stability conditions of magnetite (Van Aken et al. 2005). EMP analyses of iscorite (Table 6) yield concentrations for ZnO up to 8.9 wt.% (0.62 atoms per formula unit (apfu), normalized to ten oxygen atoms) substituting for FeO, and



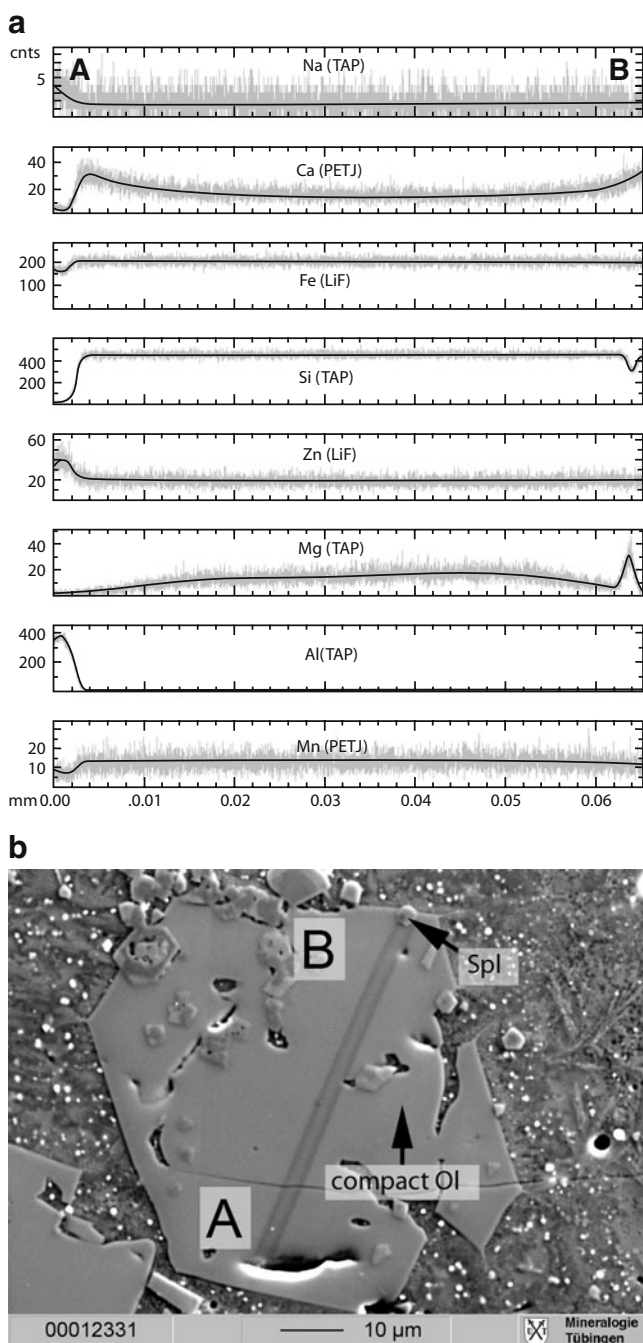


**Fig. 7** WDS profile (a) of a compact olivine. The crystal is chemically homogeneous except for Ca (enriched in rim) and Mg (enriched in core). The BSE image (b) shows the scanned grain

$\text{Al}_2\text{O}_3$  concentrations up to 4.3 wt.% (0.48 apfu) substituting for  $\text{Fe}_2\text{O}_3$ . High ZnO contents in iscorite seem to be typical of historic smelting slags (see Eggers 1999 for more analyses), but the  $\text{Al}_2\text{O}_3$  contents are, according to our knowledge, among the highest recorded in smelting slags yet.

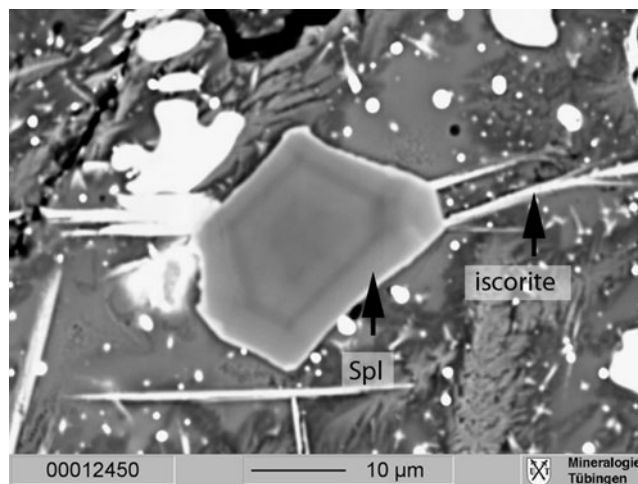


**Fig. 8** BSE images of zoned spinel crystals. Growth zonation with oriented iscorite intergrowth

### Leucite

Leucite is always found as anhedral crystals (Fig. 11) and is, together with wüstite, always the last mineral to crystallize. Eutectic exsolutions of leucite and restite–melt are common (Fig. 11), exsolutions of leucite and wüstite are rare. Leucite is a particularly interesting phase in the Wiesloch slags, because unlike all other phases it is Zn-free (no Zn was found in a WDS-scan) and has a good fitting stoichiometry. In most cases, there is just a slight over-occupation of the T2-site ( $\text{Al}+\text{Fe}^{3+} = 1.06 \pm 0.05$  apfu) and a slight under-occupation of the T1-sites ( $\text{Si}+\text{Ti}+\text{P} = 0.97 \pm 0.08$  apfu). It contains small amounts of Fe (up to 2.62 wt.% (0.07 apfu), calculated as  $\text{Fe}^{3+}$ ), Ca (up to 1.68 wt.% (0.07 apfu)), Na (up to 1.04 wt.% (0.07 apfu)), and Ba (up to 6.3 wt.% (0.09 apfu); Table 7).

### Wüstite

Wüstite forms no euhedral crystals but occurs as dendritic aggregates or as small spheres. The spheres are rare and usually crystallize early; the dendrites are common and a late or the last phase to crystallize. The most common impurities are Al (<6.88 wt.% (<0.09 apfu)) and Zn (<13.19 wt.% (<0.12 apfu) Table 8).

### Hyalophane

Hyalophane was only found in two samples. It forms long laths or double-laths, which remind of twins. In the samples in which hyalophane occurs, it is the first phase to crystallize. The only important impurity is Fe (3.21 wt.% (0.10–0.13 apfu  $\text{Fe}^{3+}$ ), Table 9).

**Table 5** Selected EMP analyses of spinels

Sample	b6 rim	b6 core	b8 rim	b8 core	b9 rim	b9 core	b12 rim	b12 core	b13 core in olivine	b14 core in olivine	b18 core in olivine	b20 core in olivine	c20 core in olivine
wt.% oxides													
SiO <sub>2</sub>	1.86	1.21	1.71	1.17	1.49	1.42	1.25	0.99	1.13	0.80	0.66	0.80	1.23
FeO	43.9	41.9	47.4	35.1	47.5	39.7	49.1	34.8	36.4	32.3	36.8	34.3	43.5
MgO	0.16	0.72	0.14	0.81	0.15	0.78	0.12	0.81	0.87	0.88	0.85	0.90	0.41
Al <sub>2</sub> O <sub>3</sub>	33.0	36.3	30.6	42.3	30.4	38.2	29.8	41.8	40.5	43.8	41.0	42.8	36.2
TiO <sub>2</sub>	1.61	1.19	1.67	0.86	1.69	1.08	1.85	0.86	1.03	0.74	0.96	0.77	1.73
ZnO	18.1	17.6	17.3	19.3	17.3	18.4	16.9	19.7	18.3	20.4	18.6	19.4	15.7
MnO	0.08	0.10	0.10	0.11	0.11	0.10	0.10	0.11	0.12	0.09	0.11	0.13	0.09
CaO	0.08	0.06	0.12	0.07	0.09	0.07	0.05	0.05	0.05	0.03	0.04	0.03	0.07
Total	98.83	99.04	99.04	99.82	98.83	99.77	99.21	99.23	98.41	99.08	98.95	99.18	99.00
mol.% spinel-endmembers													
Magnetite	28.63	26.15	33.30	17.64	33.85	23.20	35.26	18.39	19.40	15.93	20.24	17.56	24.75
Gahnite	46.06	43.08	44.14	45.92	44.06	44.67	42.45	46.87	44.24	48.01	43.92	45.76	38.61
Ulvöspine	4.18	2.97	4.34	2.08	4.38	2.67	4.75	2.09	2.54	1.77	2.30	1.84	4.32
Hercynite	21.14	27.80	18.22	34.36	17.71	29.47	17.55	32.64	33.81	34.29	33.30	34.83	32.32
Spinel	<0.01	<0.01	<0.01	<0.01	<0.01	<0.01	<0.01	<0.01	<0.01	<0.01	0.24	<0.01	<0.01
Galaxite	<0.01	<0.01	<0.01	<0.01	<0.01	<0.01	<0.01	<0.01	<0.01	<0.01	<0.01	<0.01	<0.01
Sum	100.0	100.0	100.0	100.0	100.0	100.0	100.0	100.0	100.0	100.0	100.0	100.0	100.0

### Speiss

Speiss is an usually unwanted by-product in non-ferrous metal smelting. It is composed of various intermetallic compounds. Two types of speiss can be distinguished (Thornton et al. 2009): Ferrous speiss, which is composed of Fe–As phases, and base-metal speiss, which is a mixture of Cu-, Ni-, Fe-, Ag-, Pb-arsenides and -antimonides. Thornton et al. (2009) defines a ferrous speiss as a speiss with a base-metal content of < 2–3%. The Wiesloch speisses are below this limit. They occur in two forms: Either as very

small (<1 mm) droplets, suspended in the slag, or as irregularly shaped aggregates of 5–30 mm diameter.

The phases present are

- Fe<sub>2</sub>As is the most common phase. It forms long laths, which do not show straight grain boundaries (Fig. 12).
- FeAs, the Fe-endmember of westerveldite is found relatively often in one sample (15G) but is always heavily oxidized. All other samples contain only very small amounts of FeAs.
- Löllingite was rarely found in sample 15C.

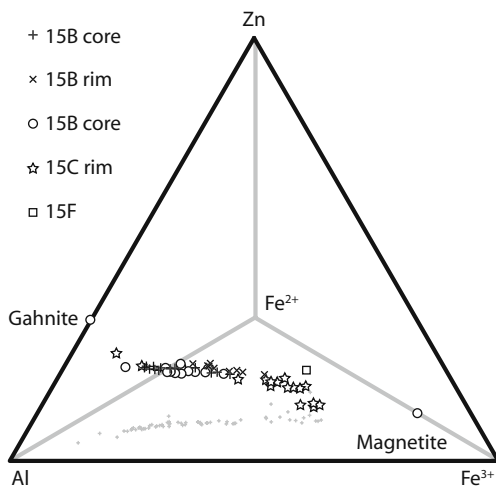


**Fig. 9** Compositional trend of spinels during crystallization. Early spinels (*cores*) are gahnite-rich, late ones (*rim*s) magnetite-rich

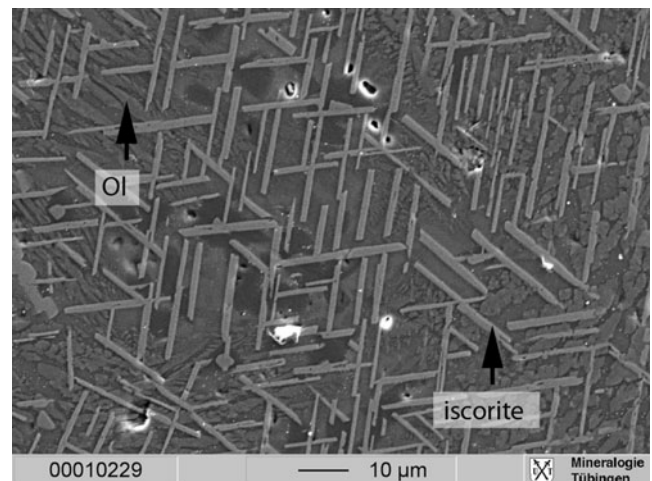


**Fig. 10** SE image of oriented iscorites

**Table 6** Selected EMP analyses of iscorite

Sample	B11_3	B12_3	B15_3	C1	C1_2	C1_4	C1_14	C1_15	C1_16	C1_17	F_2	B2_1	Iscorite ideal
wt.% oxides													
SiO <sub>2</sub>	9.25	9.41	9.95	8.81	9.51	9.51	9.83	9.80	10.14	10.83	11.14	9.44	10.38
FeO	75.0	75.4	74.7	77.6	77.2	75.4	76.9	77.6	76.6	75.5	72.9	74.2	86.9
MgO	0.11	0.55	0.79	0.60	0.54	0.53	0.52	0.43	0.45	0.46	2.44	0.20	–
Al <sub>2</sub> O <sub>3</sub>	3.46	2.71	3.16	2.12	2.05	2.96	2.30	2.69	2.34	1.94	3.20	4.31	–
TiO <sub>2</sub>	0.66	0.46	0.55	0.02	0.05	0.08	0.08	0.28	0.18	0.01	0.66	0.75	–
ZnO	8.57	8.14	7.71	7.82	7.48	8.62	7.63	6.72	7.41	7.36	6.77	8.00	–
MnO	0.15	0.17	0.22	0.05	0.05	0.08	0.08	0.06	0.08	0.06	0.35	0.16	–
CaO	0.22	0.24	0.23	0.07	0.17	0.08	0.10	0.12	0.18	0.15	0.51	0.20	–
Total	97.4	97.1	97.3	97.1	97.0	97.3	97.4	97.7	97.4	96.3	98.0	97.3	97.2
apfu (normalized to 8 cations)													
Si	0.89	0.90	0.95	0.85	0.92	0.91	0.94	0.94	0.97	1.05	1.04	0.90	1.00
Fe	4.28	4.24	4.29	4.20	4.29	4.22	4.32	4.40	4.37	4.44	4.20	4.33	5.00
Fe <sup>3+</sup>	1.74	1.82	1.67	2.06	1.93	1.83	1.84	1.79	1.77	1.68	1.48	1.60	2.00
Mg	0.02	0.08	0.11	0.09	0.08	0.08	0.07	0.06	0.06	0.07	0.34	0.03	–
Al	0.39	0.31	0.36	0.24	0.23	0.33	0.26	0.30	0.26	0.22	0.35	0.49	–
Ti	0.05	0.03	0.04	0.00	0.00	0.01	0.01	0.02	0.01	0.00	0.05	0.05	–
Zn	0.61	0.58	0.54	0.56	0.53	0.61	0.54	0.47	0.52	0.53	0.47	0.56	–
Mn	0.01	0.01	0.02	0.00	0.00	0.01	0.01	0.01	0.01	0.01	0.03	0.01	–
Ca	0.02	0.02	0.02	0.01	0.02	0.01	0.01	0.01	0.02	0.02	0.05	0.02	–
Sum	8.00	8.00	8.00	8.00	8.00	8.00	8.00	8.00	8.00	8.00	8.00	8.00	8.00
Fe <sup>3+</sup> corrected wt.% oxides													
SiO <sub>2</sub>	9.25	9.41	9.95	8.81	9.51	9.51	9.83	9.80	10.14	10.83	11.14	9.44	10.38
FeO	53.31	52.77	53.81	52.06	53.24	52.55	53.86	55.17	54.54	54.76	53.92	54.18	62.04
Fe <sub>2</sub> O <sub>3</sub>	24.07	25.12	23.22	28.36	26.60	25.35	25.58	24.88	24.51	23.02	21.11	22.30	27.58
MgO	0.11	0.55	0.79	0.60	0.54	0.53	0.52	0.43	0.45	0.46	2.44	0.20	0.00
Al <sub>2</sub> O <sub>3</sub>	3.46	2.71	3.16	2.12	2.05	2.96	2.30	2.69	2.34	1.94	3.20	4.31	0.00
TiO <sub>2</sub>	0.66	0.46	0.55	0.02	0.05	0.08	0.08	0.28	0.18	0.01	0.66	0.75	0.00
ZnO	8.57	8.14	7.71	7.82	7.48	8.62	7.63	6.72	7.41	7.36	6.77	8.00	0.00
MnO	0.15	0.17	0.22	0.05	0.05	0.08	0.08	0.06	0.08	0.06	0.35	0.16	0.00
CaO	0.22	0.24	0.23	0.07	0.17	0.08	0.10	0.12	0.18	0.15	0.51	0.20	0.00
Total	99.80	99.57	99.64	99.91	99.68	99.75	99.98	100.16	99.83	98.58	100.11	99.53	100.00

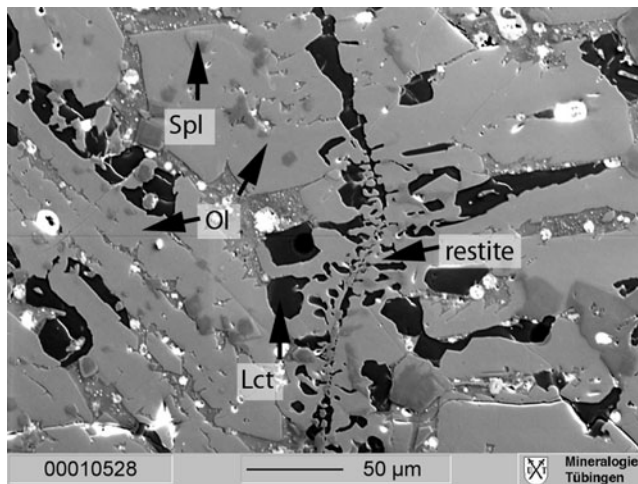


**Fig. 11** SE image of leucite-rich slag. The image shows spinifex-textured olivines, some spinels, leucite (*dark areas*), and speiss-aggregates (*bright spots*)

- Troilite is stoichiometric in the speiss and occurs as small aggregates of approximately 5–15 μm diameter. The FeS melt exsolved from the speiss melt before any crystallization began. The drops arranged themselves in

trails or domains (Fig. 12), which cross all other phases in the speiss without any reaction feature.

- In one sample (S8b), laths of metallic As were found, which tarnished within hours after polishing. There are also eutectic exsolutions of Fe<sub>2</sub>As and a restite, which are too small for EMP analysis.

#### *Matte (exsolved non-ferrous metal sulfide melt)*

In most non-ferrous metal smelting slags, speiss and matte, if present, are found together, or matte is found alone. The Wiesloch slags are an exception, since they contain only, and almost always, speiss. In material from collections or construction pits, only one single piece of matte was found, which has a diameter of ~3–4 μm and a composition close to PbS.

#### *Metallic Pb and Sb*

Metallic lead can be found either as very small aggregates (<10 μm) suspended in the slag or, more often, on or near

**Table 7** Representative EMP analyses of leucite

Sample	C_3	C_8	C_10	C_11	C_14	C_15	A_4	A_8	A_9	A_11	_12	A_13
Beam diameter	5μm	5μm	5μm	5μm	5μm	5μm	5μm	10μm	10μm	10μm	10μm	10μm
wt.% oxides												
SiO <sub>2</sub>	54.0	53.6	54.6	53.0	54.2	53.9	49.1	50.8	51.0	52.0	51.6	52.2
Fe <sub>2</sub> O <sub>3</sub>	1.35	1.50	1.03	2.62	1.60	2.48	2.32	2.01	1.94	1.35	1.89	1.08
Na <sub>2</sub> O	0.46	0.62	0.33	1.05	0.79	0.49	0.38	0.22	0.21	0.21	0.22	0.22
K <sub>2</sub> O	18.6	19.1	19.5	18.1	18.6	18.1	17.2	18.2	18.9	18.8	18.2	19.0
BaO	3.02	2.24	2.44	1.44	2.26	2.43	6.30	4.96	4.61	4.19	4.64	4.16
Al <sub>2</sub> O <sub>3</sub>	22.8	23.0	23.1	23.0	22.8	22.4	24.0	24.0	23.9	23.6	23.5	23.9
TiO <sub>2</sub>	0.09	0.07	0.05	0.03	0.06	0.05	0.20	0.14	0.13	0.09	0.14	0.10
P <sub>2</sub> O <sub>5</sub>	0.04	bd	0.02	0.05	0.10	0.06	0.04	0.03	bd	0.09	0.15	0.03
CaO	0.12	bd	bd	0.08	0.06	0.26	0.41	0.33	0.07	0.20	0.50	0.03
Total	100.4	100.1	101.0	99.4	100.5	100.2	100.0	100.7	100.8	100.4	100.7	100.8
apfu (normalized to 8 oxygen)												
Si	1.99	1.97	1.99	1.96	1.98	1.99	1.88	1.91	1.91	1.94	1.92	1.94
Fe <sup>2+</sup>	0.04	0.04	0.03	0.07	0.04	0.07	0.07	0.06	0.05	0.04	0.05	0.03
Na	0.03	0.04	0.02	0.08	0.06	0.04	0.03	0.02	0.02	0.02	0.02	0.02
K	0.87	0.90	0.91	0.85	0.87	0.85	0.84	0.87	0.91	0.89	0.87	0.90
Ba	0.04	0.03	0.03	0.02	0.03	0.04	0.09	0.07	0.07	0.06	0.07	0.06
Al	0.99	1.00	0.99	1.00	0.99	0.97	1.08	1.06	1.06	1.04	1.03	1.04
Ti	0.00	0.00	0.00	0.00	0.00	0.00	0.01	0.00	0.00	0.00	0.00	0.00
P	0.00	–	0.00	0.00	0.00	0.00	0.00	0.00	–	0.00	0.00	0.00
Ca	0.00	–	–	0.00	0.00	0.01	0.02	0.01	0.00	0.01	0.02	0.00
Sum	3.97	3.99	3.98	4.00	3.98	3.96	4.01	4.00	4.02	3.99	3.99	3.99



**Table 8** EMP analyses of wüstites

Sample	wu_f9	wu_fl3	wu_fl5	wu_b3	wu_b11	wu_b12	wu_b13	wu_al	wu_a3	wu_a10	wu_e12	wu_e13	wu_e14
wt.% elements													
Si	0.15	0.21	0.16	0.35	0.27	0.27	0.60	0.19	0.19	0.17	0.19	0.16	0.19
Fe	70.2	70.6	70.1	65.5	64.8	67.0	62.8	66.2	68.9	68.1	67.7	67.6	68.4
Mg	1.84	1.56	2.08	0.00	0.03	0.03	0.00	0.52	0.24	0.46	0.27	0.26	0.23
Al	0.22	0.14	0.27	0.27	0.11	0.47	0.58	0.25	0.11	0.18	0.39	0.34	0.27
Ti	0.08	0.03	0.10	0.12	0.05	0.21	0.26	0.27	0.04	0.19	0.20	0.18	0.16
Zn	2.76	2.95	2.63	8.64	8.57	7.59	9.94	7.77	5.51	5.61	6.37	6.50	6.16
Mn	0.09	0.11	0.09	0.07	0.09	0.10	0.05	0.52	0.39	0.43	0.22	0.23	0.23
Ca	0.11	0.21	0.15	0.13	0.13	0.06	0.27	0.29	0.40	0.34	0.22	0.20	0.19
O	24.0	24.2	24.3	24.4	24.7	23.6	24.9	23.6	24.1	23.9	24.0	23.9	24.0
Total	99.5	100.0	99.8	99.5	98.8	99.4	99.4	99.6	99.9	99.4	99.6	99.4	99.8
apfu normalized to 1 cation													
Si	0.00	0.01	0.00	0.01	0.01	0.01	0.02	0.00	0.00	0.00	0.00	0.00	0.00
Fe <sup>2+</sup>	0.78	0.76	0.77	0.64	0.46	0.77	0.60	0.75	0.71	0.73	0.73	0.73	0.73
Fe <sup>3+</sup>	0.11	0.15	0.12	0.24	0.42	0.11	0.23	0.11	0.19	0.16	0.15	0.16	0.16
Mg	0.05	0.05	0.06	0.00	0.00	0.00	0.00	0.02	0.01	0.01	0.01	0.01	0.01
Al	0.01	0.01	0.01	0.01	0.01	0.03	0.03	0.01	0.01	0.01	0.02	0.02	0.01
Ti	0.00	0.00	0.00	0.00	0.00	0.00	0.00	0.00	0.00	0.00	0.00	0.00	0.00
Zn	0.03	0.03	0.03	0.10	0.10	0.08	0.11	0.09	0.06	0.06	0.07	0.07	0.07
Mn	0.00	0.00	0.00	0.00	0.00	0.00	0.00	0.01	0.01	0.01	0.00	0.00	0.00
Ca	0.00	0.00	0.00	0.00	0.00	0.00	0.00	0.01	0.01	0.01	0.00	0.00	0.00
Sum	1.00	1.00	1.00	1.00	1.00	1.00	1.00	1.00	1.00	1.00	1.00	1.00	1.00

**Table 9** EMP analysis of hyalophane

Sample	S8ACls_4	S8ACls_6	15K_hy_1	15K_hy_7	15K_hy_8	15K_hy_9	15K_hy_11
wt.% oxide							
SiO <sub>2</sub>	40.7	37.2	50.5	51.4	52.2	50.4	52.3
Fe <sub>2</sub> O <sub>3</sub>	3.2	4.9	2.6	2.6	2.3	3.0	2.5
Na <sub>2</sub> O	0.09	0.09	0.31	0.31	0.34	0.30	0.35
K <sub>2</sub> O	3.91	2.67	8.77	8.87	9.16	8.65	9.15
BaO	29.3	31.8	16.9	16.7	16.2	17.0	15.6
Al <sub>2</sub> O <sub>3</sub>	23.7	22.8	21.0	20.9	20.9	20.9	20.7
TiO <sub>2</sub>	0.65	0.77	0.42	0.44	0.41	0.45	0.41
P <sub>2</sub> O <sub>5</sub>	0.04	0.09	0.03	0.05	0.01	0.05	0.05
CaO	0.18	0.32	0.30	0.41	0.27	0.40	0.69
Total	101.8	100.6	100.9	101.7	101.7	101.1	101.7
mol.% endmembers							
Celsiane	0.65	0.73	0.34	0.34	0.32	0.34	0.31
Orthoklase	0.28	0.20	0.58	0.58	0.59	0.57	0.59
Anortite	0.01	0.02	0.02	0.02	0.01	0.02	0.03
Albite	0.01	0.01	0.03	0.03	0.03	0.03	0.03
Sum	0.95	0.96	0.97	0.97	0.95	0.96	0.96

the interface between speiss and slag (Fig. 13). The lead appears to be homogeneous on freshly polished surfaces. Tarnishing was observed after a few days. The lead is relatively pure, containing an average of 99.2 wt.% Pb, but it can contain up to 1.04 wt.% Mg, 0.83 wt.% Sb, 0.31 wt.% Bi, 0.23 wt.% Cd, 0.16 wt.% Fe, and 0.01 wt.% Zn. Ag was not found in a WDS-scan. Occasionally, small (up to 4  $\mu$ m) euhedral crystals of metallic antimony can be found in the lead.

The antimony crystals contain also very few impurities ( $\leq 0.02$  wt.% Fe,  $\leq 0.01$  wt.% Zn, and Mg and  $\leq 1.8$  wt.%

Pb) which may, however, be an analytical artifact due to the small size of the crystals.

#### Ores from Wiesloch

As shown by Pfaff et al. (2010), the mineralization in Wiesloch can be subdivided into four stages: a diagenetic pre-ore stage which shows small crystals of pyrite and chalcopyrite in fractures together with dolomite and calcite. Ore stage I is represented by galena crystals on fractures and galena as well as sphalerite impregnations. In ore stage II, colloform sphalerite is dominant, which includes euhedral galena and sulfosalts as jordanite and geocronite.

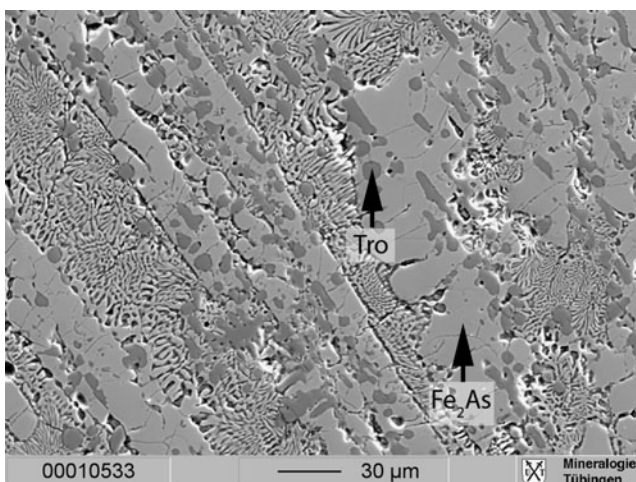


**Fig. 12** Typical speiss-texture with long Fe<sub>2</sub>As-laths, eutectic exsolution of Fe<sub>2</sub>As, and restite, the dark gray drops are FeS trails. SE image

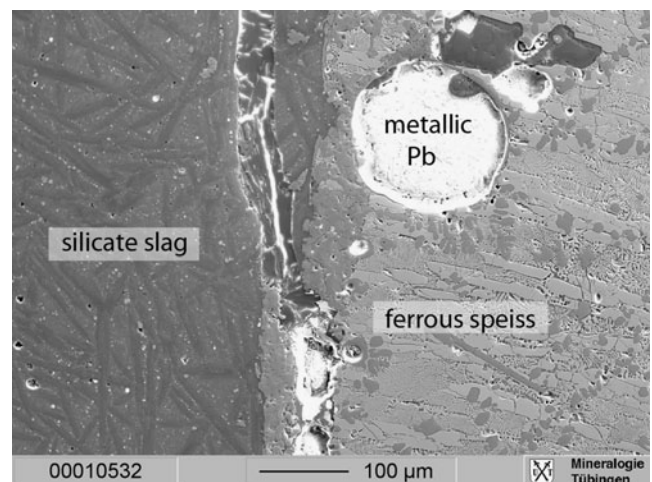


**Fig. 13** SE image of metallic lead in speiss at the contact to silicate slag

Both ore stages are accompanied by colloform pyrite. As last stage (post-ore) another generation of calcite and barite precipitated. Some representative ore analyses are given in Table 10. For a detailed description of the mineralization, see Pfaff et al. (2010).

The ores described therein come from geological collections. It must be kept in mind that all the high-grade ores were exploited in the past, and so the leftovers and the mineralization found today do not necessarily represent the material mined in former times. Thus, assessments on the quantity of metal (especially silver) recovered from the deposit cannot be based on the present data due to the risk of underestimation. Usually, the silver-bearing mineral in MVT deposits is galena. However, in Wielsoch, galena only bears very little silver (median usually below detection limit of 0.014 wt.%). In contrast, sphalerite can contain 0.03–0.05 wt.% silver (median, equivalent to 300–50 g/t). This silver content is preserved during the weathering process, so the galmei from Wiesloch contains also considerable amounts of silver up to 0.015 wt.% (150 g/t).

#### Bulk composition of the slags

Volatile elements, specifically Zn and S, escape with the fumes released during the smelting process. More of these elements were evaporated during melting for the production of the quenched beads (B1). This means that in any case, the ZnO and SO<sub>2</sub> contents in the slag can only provide minimum estimate for the bulk charge. This is why B1 was

only used to estimate the liquidus temperature of the material.

To obtain reliable bulk analyses, the second batch (B2) of quenched beads was made. Using the same analysis routine as with B1, the samples yielded totals of 73–83 wt.%. Taking into account the mass of “Spectromelt” flux added to the sample, the totals of the analyses rise to ~100 wt.%. For interpretation of the data, Li<sub>2</sub>O and B<sub>2</sub>O<sub>3</sub> were ignored, and the analyses were normalized to 100 wt.%.

The bulk compositions of the analysed samples are quite variable. Generally, the SiO<sub>2</sub>-content can be used to group samples. One group shows SiO<sub>2</sub>-contents of about 40 wt.%, while the second has only 25–30 wt.% SiO<sub>2</sub>. Something similar occurs in the Al<sub>2</sub>O<sub>3</sub>-contents: One group shows values of 5 wt.%, and the other shows values of 7.5–9 wt.%, respectively. The SiO<sub>2</sub> and Al<sub>2</sub>O<sub>3</sub> groups are uncorrelated; in general, no constant element ratios were not observed observable. The bulk composition of all samples is presented in Table 11.

#### Melt properties

In this section, the liquidus temperature and viscosity of the slag will be addressed. Observations from the melting experiments and the bulk chemistry data will be used to estimate and calculate these values.

It must be kept in mind that temperature and viscosity were the prime variables for the historic smelters. It is also important to think about the purpose of slag: It is (1) to

**Table 10** EMP analyses of ores (Pfaff et al. 2010)

	Galena	Pb–As–Sb sulfosalts	Crystalline sphalerite	Colloform sphalerite	Pyrite
S	13.64	17.94	32.87	32.75	49.46
As	bd	6.65	0.09	0.07	6.23
Sb	2.41	3.89	0.01	bd	0.01
Bi	bd	bd	–	–	–
Pb	83.76	69.65	–	–	–
Zn	bd	bd	66.55	67	0.38
Cd	bd	bd	bd	bd	–
Fe	0.03	0.02	0.01	0.01	42.65
Hg	0.08	0.03	–	–	–
Cu	bd	bd	bd	bd	0.08
Ag	bd	bd	0.03	0.02	bd
Tl	0.05	0.33	bd	bd	0.98
Mn	–	–	bd	bd	bd
Cl	–	–	0.19	0.05	–
Ni	–	–	–	–	bd
Co	–	–	–	–	bd
Sum	99.97	98.51	99.75	99.9	99.78

gather impurities from the charge, (2) to prevent the metal from being reoxidized, and (3) to separate the “clean” metal from the “unclean” charge. To reach a slag composition with a low liquidus has several advantages:

(1) The amount of fuel that is needed to keep the slag fluid can be kept lower. (2) The lower the temperature is, the lower is the metal loss by evaporation. (3) The reduction process starts working at an adequate speed at  $\sim 800^\circ\text{C}$  (Goldenberg et al. 1996), so for the reduction, no higher temperatures are needed. (4) The furnace lining will be more affected by high temperatures. (5) As soon as the temperature drops under the liquidus temperature of the slag, crystallization starts and the viscosity rises significantly (Pawlek 1983).

A low viscosity is essential for an effective smelting process: (1) Only low viscosity slags can be removed quickly from the furnace without temperature loss that would cause the interruption of the reduction process or result in the solidification of the slag inside the furnace. (2) The lower the viscosity of the slag, the faster it can adjust its shape to the changing geometry in the furnace and ensure a stern separation of charge and metal. (3) Reduced metal drops can pass the slag column quickly, which increases the metal recovery significantly.

#### Experimental determination of liquidus temperatures

The aperture in the graphite tube furnace allowed the observation of the samples while melting. The melting temperature could be estimated by monitoring the sample and the control unit simultaneously. As soon as the solidus was exceeded, a fining of the sample surface, agglomeration, and slow formation of a spheroid were observed. Solidus temperatures varied from  $\sim 875^\circ\text{C}$  to  $\sim 950^\circ\text{C}$ .

In most samples, a fast rotational or convective movement and a rapid change of the shape to a sphere- or lens-like shape could be observed, when the sample exceeded the liquidus. Liquidus temperatures of the samples are between  $\sim 950^\circ\text{C}$  and  $\sim 1,100^\circ\text{C}$ . To confirm this, three samples were molten in  $100^\circ\text{C}$  steps from  $800^\circ\text{C}$  to  $1,400^\circ\text{C}$ . The textures of the resulting quenched beads were observed microscopically. They showed that some samples were completely glassy after melting at  $1,000^\circ\text{C}$ ; the majority of samples were molten completely at  $1,100^\circ\text{C}$ .

#### Viscosity

The viscosity of the slag melt was calculated using three models (Pawlek 1983; Bachmann et al. 1989; Battle and Hager 1990). They use the same mathematical approach but different constraints. All equations include a “slag viscosity index” ( $K_Z$  in Pawlek 1983;  $K$  in Endell et al.

1932 as cited in Bachmann et al. 1989) or “weight parameter” (WP in Battle and Hager 1990) which is the ratio of viscosity-lowering to viscosity-increasing oxides. A viscosity is calculated from this index by regression, which is calibrated against the data from viscosity measurement experiments.

Pawlek (1983) applied a mass correction (not displayed here) to every oxide and discriminates between bivalent and trivalent iron. The equation is valid only for a temperature of  $1,150^\circ\text{C}$  and is limited to a specific range of  $K_Z$

$$K_Z = (\text{FeO} + \text{MnO} + \text{MgO} + \text{ZnO}) / (\text{SiO}_2 + \text{Al}_2\text{O}_3 + \text{Fe}_2\text{O}_3 + \text{CaO}) \quad (1)$$

$$\eta(1,150^\circ\text{C}) = 0.44/K_Z^2 - 1.55[\text{Pa s}] \text{ for } K_Z = 1.4 - 2.0 \quad (2)$$

$$\eta(1,150^\circ\text{C}) = 0.2 - 0.01 \times K_Z[\text{Pa s}] \text{ for } K_Z = 2 - 3 \quad (3)$$

Bachmann et al. (1989) took more oxides into account. All iron was assumed as bivalent in their equation. From the resulting slag viscosity index, a temperature-dependent viscosity is calculated by linear regression. Except for temperature, no boundary conditions are given.

$$K_Z = (\text{CaO} + \text{MgO} + \text{FeO} + \text{MnO} + \text{TiO}_2 + \text{ZnO} + \text{PbO} + \text{K}_2\text{O} + \text{Na}_2\text{O} + \text{SO}_2) / (\text{SiO}_2 + \text{Al}_2\text{O}_3 + \text{P}_2\text{O}_5) \quad (4)$$

$$\ln(\eta) = 26.46 - 23.67 \times (0,001 \times T) - 3.12 \times K_Z + 0.59 \times K_Z^2 + 3.84 \times (0.001T)^3 \quad (5)$$

The equation of Battle and Hager (1990) combined the “weight parameter” (WP) (which is equivalent to the slag viscosity index) with six temperature-dependent factors  $A_0$ – $A_5$ . The calculations are limited in temperature range, chemical composition, and the range of WP, which is defined as

$$\text{WP} = (\text{CaO} + \text{MgO} + \text{ZnO} + \text{PbO} + \text{CuO} + \text{FeO} + \text{Fe}_2\text{O}_3 + \text{CaS}) / (\text{SiO}_2 + \text{Al}_2\text{O}_3) \quad (6)$$

$$\eta = A_0 + \text{WP} \times A_1 + \text{WP}^2 \times A_2 + \text{WP}^3 \times A_3 + \text{WP}^4 \times A_4 + \text{WP}^5 \times A_5 \quad (7)$$



**Table 11** Bulk composition of Wiesloch slags

Sample Bead no.	15-5 Q2_2	15-E Q3_5	15-g Q4_5	15-19 Q5_5	15-8 Q8_3	15-J Q9_5	15-13 Q10_5	15-10 Q11_1	15-18 Q12_5	15-1 Q13_4	15-20 Q14_5	15-F Q15_3	15-17 Q16_1	15-B Q17_2	15-S8A Q18_5	K <sub>glass</sub>
wt.% oxide																
SiO <sub>2</sub>	32.4	32.2	33.1	38.8	43.6	30.0	32.1	32.7	42.7	32.1	42.0	43.0	26.9	31.6	28.2	39.2
FeO	38.8	41.0	36.3	32.5	22.8	47.4	40.7	27.1	26.7	34.1	25.9	21.0	36.8	45.0	37.6	21.5
Al <sub>2</sub> O <sub>3</sub>	6.0	5.4	5.9	9.4	5.0	5.8	5.4	5.6	7.2	7.3	7.5	5.4	6.1	7.3	5.7	5.3
ZnO	5.1	5.7	5.9	5.3	10.0	4.5	6.2	20.8	5.4	17.4	7.4	8.8	18.4	8.1	6.3	11.3
CaO	10.1	9.9	11.2	5.1	12.7	6.1	10.7	8.0	8.9	2.8	8.8	15.8	4.6	3.8	4.7	8.5
MgO	1.41	1.20	2.10	1.98	1.05	1.81	0.76	0.95	2.51	0.96	1.88	1.15	0.87	0.87	1.02	1.59
MnO	0.65	0.60	1.04	0.09	0.35	0.41	0.76	0.46	0.36	0.33	0.41	0.31	0.33	0.36	0.34	0.33
BaO	1.71	0.64	2.12	0.80	0.96	1.44	0.98	0.80	2.03	1.17	2.22	0.85	2.88	0.18	10.05	4.17
TiO <sub>2</sub>	0.27	0.27	0.31	0.31	0.21	0.27	0.25	0.21	0.31	0.29	0.32	0.23	0.28	0.21	0.45	0.32
K <sub>2</sub> O	1.34	1.17	1.30	1.85	1.45	1.14	1.07	0.88	1.59	1.27	1.70	1.16	1.02	1.16	1.13	1.76
SO <sub>2</sub>	1.39	0.56	0.02	1.48	0.32	0.41	0.22	0.40	1.03	0.35	0.93	0.20	0.59	0.35	4.02	0.59
P <sub>2</sub> O <sub>5</sub>	0.68	0.63	0.53	1.28	1.07	0.53	0.75	0.99	0.67	0.68	0.93	1.14	0.93	0.65	0.45	1.24
PbO	0.14	0.79	0.18	1.04	0.42	0.23	0.12	1.19	0.52	1.31	0.10	0.86	0.35	0.47	0.08	4.60
Total	100.00	100.00	100.00	100.00	100.00	100.00	100.00	100.00	100.00	100.00	100.00	100.00	100.00	100.00	100.00	100.49

Analyses are normalized to 100% after removal of Spectromelt-flux. The sample K<sub>glass</sub> is a glassy slag and was measured directly

Using Pawleks (1983) formula, only 29 of 84 data points are within the limits of the formula. The remaining 55 data points are below the lower limit of  $K_Z = 1.4$ . It yields viscosity values of 0.2 to 2.9 Pa s at a fixed temperature of 1,150°C, which fits the observations very well.

The model of Bachmann et al. (1989) theoretically covers all melt compositions but was calibrated on low-Fe slags. At a temperature of 1,400°C, we calculated values of 0.8 to 18.7 Pa s. The equation yields values of 14.0 to 311.4 Pa s at 1,150°C, which seems to be unrealistic for smelting (Pawlek 1983). So for the experiments at 1,400°C, the equation matches the observations but at lower temperatures, which were arguably realized in the smelting process; it does not seem to be applicable.

Despite the numerous restrictions, the equation of Battle and Hager (1990) covers the interesting temperature range as well as the full range of compositional variation. The temperature-dependent term yields values of 0.5 to 6.7 Pa s at 1,350°C and 2.2 to 31.0 Pa s at 1,150°C, respectively. The calculated results and the viscosities of some other liquids for comparison are shown in Tables 12 and 13, respectively.

*Bloomery experiment*

When tapping the furnace at the end of the process, a cavity and a hard silicate plug were found at the bottom of the furnace. The plug was sintered to the furnace wall just above the tuyère level and did not give way to the charge, so the charge was held above the tuyères. Because of the hardness and size of the plug, it was not possible to remove it without destroying the furnace.

Unexpectedly, all the lining and a part of the bricks behind it were dissolved in a zone of ~15–20-cm height just above the silicate plug (Fig. 2b). Within the silicate plug, we found a zone where the unaltered red furnace lining was followed by black sintered lining. The next zone consisted of green to brownish glass with quartz grains (originating from the sand) in it. Adhered to this sequence, we found a silicate slag with some aggregates of metallic iron in it. This sequence was sampled in order to get the information on the interaction process of the slag and the furnace lining (Fig. 2d).

EMP analyses of this cross-section revealed the red and black part to be a very inhomogeneous ceramic-like material. It consists of quartz grains and a very fine-grained to glassy heterogeneous matrix. The following green glass seems to be more homogeneous. Here, we see the first interactions between the slag melt and the furnace wall: FeO as well as CaO were taken up from the slag by the green glass (Fig. 2c). The difference between the green glass and the ground mass of the slag itself is shown clearly by the elevated FeO and MgO in the slag and the disappearance of the quartz grains. The green glass bears plenty of them, the slag almost none.

Consequently, the zone of metasomatism is very narrow (<1 cm). Textures of the samples imply that bulk dissolution

**Table 12** Viscosity calculations based on different models

Quenched bead	Q2_2	Q3_5	Q4_5	Q5_5	Q8_3	Q9_5	Q10_5	Q11_1	Q12_5	Q13_4	Q14_5	Q15_3	Q16_1	Q17_2	Q18_5
Sample	15-5	15-E	15-g	15-19	15-8	15-J	15-13	15-10	15-18	15-1	15-20	15-F	15-17	15-B	15-S8A
Bachmann et al. (1989) at 1,150°C															
$K_z$	1.7	1.8	1.6	1.1	1.1	1.9	1.7	1.7	1.0	1.6	1.0	1.1	2.0	1.7	1.7
$\lg(\eta)$	1.5	1.4	1.6	2.4	2.4	1.3	1.4	1.5	2.5	1.6	2.5	2.3	1.2	1.5	1.5
$\eta$ in Pa s	33.5	26.0	37.4	224.4	233.2	19.6	26.9	34.0	296.0	42.1	286.8	205.8	16.2	33.1	29.8
Pawlek (1983) at 1,150°C															
$K_z$	1.2	1.3	1.1	0.9	0.7	1.6	1.2	1.3	0.8	1.5	0.8	0.6	1.8	1.6	1.4
Out of range			Out of range	Out of range	Out of range	0.4	Out of range	Out of range	Out of range	0.7	Out of range	Out of range	0.3	0.5	1.0
Battile (1990)															
$T$ (°C)	WP	1.7	1.6	1.1	1.1	1.8	1.7	1.6	1.0	1.5	1.0	1.1	2.0	1.6	1.6
1,150		3.1	3.8	21.7	20.4	2.7	3.1	3.4	29.2	3.9	27.9	17.0	2.3	3.4	3.8
1,200		3.0	2.3	3.1	14.1	1.9	2.3	2.7	18.4	3.3	17.9	12.4	1.7	2.7	3.2
1,250		2.3	2.0	8.4	7.9	1.9	2.0	2.1	11.1	2.4	10.7	6.8	1.9	2.2	2.4
1,300		1.7	1.4	1.8	6.7	1.1	1.4	1.6	10.6	1.8	10.0	5.4	0.9	1.6	1.8
1,350		1.6	1.4	1.7	4.8	1.1	1.4	1.6	6.4	1.7	6.2	4.2	0.8	1.6	1.7

Viscosities are given in Pa s,  $K_z$ , and WP are dimensionless and equivalent

**Table 13** Viscosities of some other liquids for comparison

Material	Viscosity in Pa s	Temperature in °C
Water	0	20
Olive oil	0.11	20
Engine oil (SEA10)	0.2	20
Grape juice	2–5	20
Honey	10	20
Peanut butter	25	20
Basaltic melt	~300	1,200

Shown are the viscosities of different materials for comparison in Table 12

of the lining by the slag is an acceptable approximation for the process reconstruction.

## Discussion

### Mineral chemistry

Fayalite slag is the most abundant slag in ancient and historical pyrometallurgical smelting. In this material, fayalite is the predominant phase in contrast to more rarely described pyroxene and melilite slags. Generally, the fayalite can contain considerable amounts of larnite (up to 50 mol. %), tephroite, and forsterite components in which case one should actually name the slag olivine slag. Furthermore, the slag can contain complex spinel solid solutions, whose composition mainly depends on the bulk chemistry of the charge (Hauptmann et al. 1988). These spinels are often rich in magnetite. Other common phases are iscorite, feldspars (typically potassic feldspar or celsiane) or leucite, wüstite, and hematite (e.g., Kronz and Eggers 2001; Bachmann 1982; Craddock et al. 1985). Pyroxenes, melilites, and other phases like rhönite can be accessory phases (Kronz et al. 1992).

In the Wiesloch slag, olivines and spinels are always early crystallizing phases. So the compositions of these phases reflect the composition of the “primary” melt. We see that the majority of the Zn and Mg in the primary melt were incorporated into these two early phases, which indicates some kind of slag “differentiation”. This differentiation is also shown by the chemical zonation of the spinels, ranging from gahnite to magnetite.

In the general spinel formula ( $A^{2+}B_2^{3+}O_4$ ), the ratio of trivalent ( $Fe^{3+}$ ,  $Al^{3+}$ ) to bivalent (Zn,  $Fe^{2+}$ , Mg, Mn) ions is 2. The Wiesloch spinels always show ratios  $<2$ , which indicates an excess of bivalent ions. Based on Wiesloch spinel analyses and using the number of trivalent ions (calculated as atoms per formula unit) as a restriction for spinel formula calculation, there is a remaining amount of

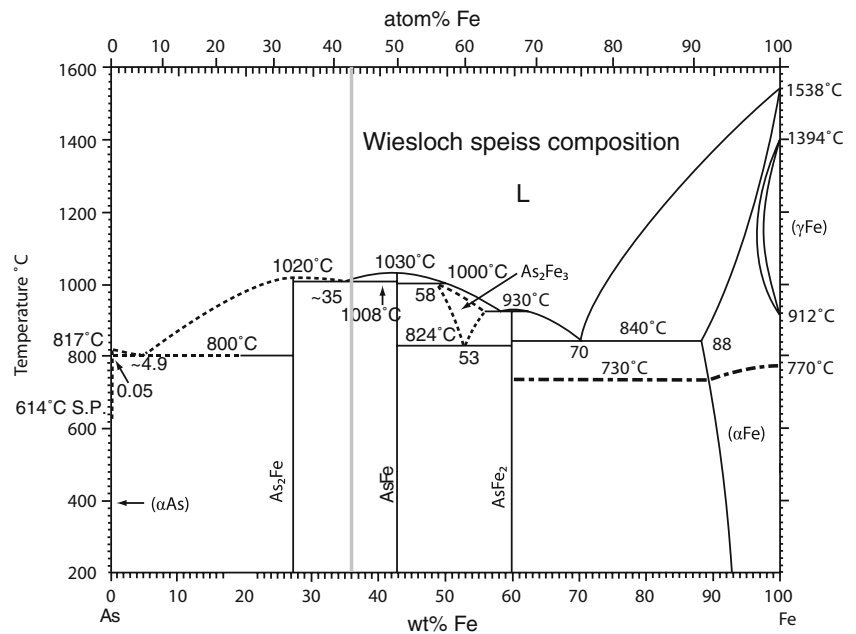
bivalent ions and Si, which cannot be attached to the spinel’s crystal lattice. The ratio of the remaining bivalent ions and the Si is exactly 2, so these elements represent an olivine composition in the system fayalite–forsterite–larnite–tephroite. The reasons for this behaviour could be the formation of a solid solution or mechanical mixing on a sub-micrometer scale. It is very likely that kinetic factors play a role in the formation of such complex spinels. This shows the non-equilibrium condition of the smelting process.

The iscorite textures in our samples are still equivocal. Some can either be interpreted as a replacement of a wüstite dendrite through iscorite or as wüstite dendrites nucleating on iscorite. However, there are also iscorites that are completely coated by wüstite, which can hardly be interpreted as a reaction of wüstite and fayalite. In most cases, there is no close spatial relationship between iscorite and wüstite. In iscorite bearing types M4 and M5 slags, there was no early wüstite identified, although Smuts (1992) states this to be necessary for the formation of iscorite. It is therefore possible that a second, yet unknown, process results in the formation of iscorite.

The wüstite from our samples is not as reduced as it theoretically should be. According to our formulae calculation ( $Fe^{3+}$  calculation after Droop 1987), it shows average  $Fe^{2+}/Fe^{3+}$  ratios of  $\sim 4.4$  with extreme values of 1.1 and 11.9. The fraction of  $Fe^{3+}$  incorporated might be the result of the cooling of the melt under slightly oxidizing conditions (in air). The results imply that at the time the wüstite dendrites crystallized, there was still some Zn in the melt. All remaining zinc was taken up by the wüstite, as leucite is Zn-free.

It is well known from other historical smelting sites that speiss can occur as lumps of several kilograms. Although speiss can be found well preserved at other smelting sites, the Wiesloch speiss seems to be unstable if exposed to air. Fresh speiss lumps start oxidizing and decomposing in air within hours (Hildebrandt, personal communication). The occurrence of speiss in smelting slags is always a problem. Its composition has been known to smelters since the early modern period (Ercker 1580), but also in the third millennium BCE smelting relics, speiss has been found (Hauptmann et al. 2003; Thornton et al. 2009). Speiss can be desilvered in a separate and complex smelting step (Ercker 1580). Unfortunately, it is unknown whether speiss formation simply occurs if the charge is rich in arsenic or antimony or if there was a “speiss technology” which enabled the smelter to produce speiss selectively to bind arsenic and antimony. Thornton et al. (2009) postulate speiss technology dating back to the third millennium BCE in Iran. Craddock et al. (1985) proposes a speiss technology in which argentiferous speiss from Rio Tinto (Spain, Roman period smelting) was desilvered. This theory was rejected by Kassianidou (1998).

**Fig. 14** Fe–As phase diagram (redrawn after Okamoto 1991). The *gray line* shows the average composition of the Wiesloch speiss



We assume the existence of a speiss technology for Wiesloch for the following reasons: (1) Arsenic can hardly be removed from the ore by roasting (Ercker 1580; Kassianidou 1998), so smelters had to find a way to precipitate it in an alloy or phase assemblage. (2) The speiss from Wiesloch is Ag-free, so there is no reason for further treatment (no Ag was found in a WDS-scan). (3) Although speiss is hard to handle, the bulk composition of the Wiesloch speiss is nearly eutectic (Fig. 14). (4) Speisses are very common in the Wiesloch slags. (5) The absence of matte points to a roasting process with a very high efficiency or multiple roasting steps of the ores, which resulted in a roasting produce almost completely devoid of sulfur. A report of a Wiesloch smelter from 1725 (Generallandesarchiv Karlsruhe 190/15, 28f.) shows that multiple roasting steps were common. We do not understand yet why the speiss did not separate from the slag melt. Probably, the slag was tapped before the segregation was complete.

#### Liquidus temperature

For comparison with the observed liquidus, the liquidus of one sample was calculated using the method of Leeman and Scheidegger (1977), which uses the Fe, Mg, or Mn distribution between olivine and glass. According to Leeman and Scheidegger (1977), the Fe-based thermometer is the one that fits best to most systems. Also in our case, the observation is reproduced in the best way by the Fe-based equation. Unfortunately, only one of the samples analysed by EMP shows glass and olivines which were large enough to be analysed by EMP. For this sample, the experimentally observed liquidus of  $\sim 1,100^{\circ}\text{C}$  and the calculated one of  $1,092 \pm 30^{\circ}\text{C}$  agrees very well. The

calculated temperature of  $1,092^{\circ}\text{C}$  is significantly below the temperatures predicted by the ternary phase diagrams. This shows that ternary phase diagrams are insufficient for the estimation of liquidus temperatures in multi-component slag systems since they do not cover all compositions. A typical slag analysis from Wiesloch plotted in ternary phase diagrams shows eutectic liquidus temperature of  $1,200^{\circ}\text{C}$  in the  $\text{SiO}_2\text{--CaO--FeO}$  system (Fig. 15),  $1,400^{\circ}\text{C}$  in the  $\text{SiO}_2\text{--Al}_2\text{O}_3\text{--CaO}$  system and  $1,720^{\circ}\text{C}$  in the  $\text{SiO}_2\text{--Al}_2\text{O}_3\text{--FeO}$  system (Osborn and Muan 1960). However, small amounts of alkalis or alkali earths can lower the liquidus temperatures to less than  $1,000^{\circ}\text{C}$  as is seen in our samples.

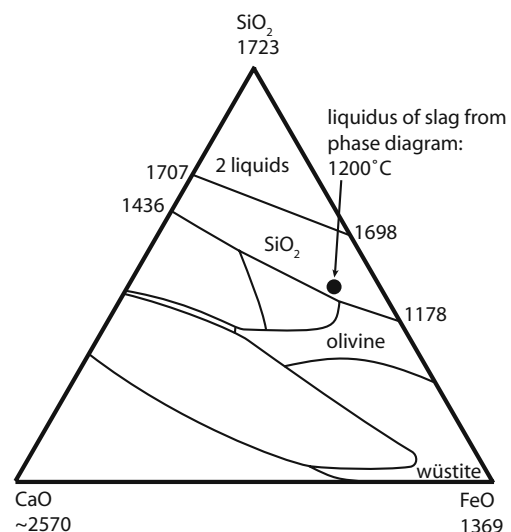


**Fig. 15** System  $\text{SiO}_2\text{--CaO--FeO}$  (redrawn after Osborn and Muan 1960) The *black spot* shows the composition of a Wiesloch slag



## Viscosity calculations

All models used yield different estimates for viscosity, which vary by two orders of magnitude. Since all models are based on experimental measurements of historic (Bachmann et al. 1989) and modern (Pawlek 1983; Bachmann et al. 1989, Battle and Hager 1990) slags of variable composition, the applicability of the models to the slags of Wiesloch is limited. Taking the fact into account that no general quantitative theory for viscosity calculations of slag systems has been formulated yet, we need to use the model that reproduces our observations from the Wiesloch slags.

The values of Pawleks (1983) equation reproduce our experimental data best, but only one third of the data meets the restrictions. The values by the Battle and Hager (1990) formula are only slightly higher than those of Pawlek (1983). Both models yield values in the same order of magnitude, and their differences should be covered by the analytical and calibration errors of the models. Taking into account that the model of Battle and Hager (1990) is only working in a certain range of chemical variability (which covers the Wiesloch slags completely), this model seems to be the most reliable. The equation of Bachmann et al. (1989) appears not to be applicable in our case.

## Ores used for smelting

Although the Wiesloch slags contain up to 23 wt.% ZnO (Table 11), the modelling allows only a minimum estimation for added Zn phases in the charge. Any ZnO added to the charge will be reduced to metallic Zn, but Zn evaporates at 907°C. So a part of the Zn will be released with the fumes of the furnace, another part will precipitate on the furnace's wall, and the rest will dissolve in the silicate melt and enter the slag minerals. Accordingly, the calculation of a Zn flux is not reasonable.

However, the high ZnO content of the slags is highly interesting because analyses of Zn ores from Wiesloch show very high Ag contents in sphalerite (usually 0.02–0.1 wt.%, up to 0.5 wt.% ppm, Pfaff et al. 2010) and metallic silver in galmei (up to 0.014 wt.%) but unexpectedly low Ag contents in galena (median below detection limit of 0.014 wt.%), which is usually the silver-bearing mineral in MVT deposits (Table 10, see Pfaff et al. 2010 for further ore analyses and range). Here, we can see that the ores that are found in Wiesloch today seem to be “low-grade” ores. It is likely that everything with higher silver content has already been mined. We also know that coins which were made from Wiesloch silver bear high amounts of Zn (~0.17–0.20 wt.%, some up to 0.8 wt.%; Ilisch et al. 2004). We therefore assume the ore used for smelting was a mixture of argentiferous galmei and galena.

## Process reconstruction

The aim of the reconstruction is to calculate the compositional range of the charges used in Wiesloch. The whole slag-system ( $S$ ) is composed of several reactants ( $R$ ). The sum of all reactants ( $R$ ) is called charge. All of these reactants contain several chemical components ( $E_i$ ). The composition of the slag depends on the composition as well as the amount of the reactants ( $R$ ). Some elements ( $E_a$ ) are brought to the slag ( $S$ ) by one of the reactants predominantly. The fraction ( $F_i$ ) of an element ( $E_a$ ) in a reactant can be used to calculate the fraction of these reactants in the slag. For a complete reconstruction of the charge, the composition of slag, the furnace lining, and the charcoal ash and the fluxes should be known. In the Wiesloch ores, no element was found that partitions completely to the slag (without loss by evaporation) and occurs only in the ores. So the following calculations consider only fluxes and major slag forming reactants (ash, furnace lining). The slag chemistry was analysed on the quenched beads. Ash compositions were taken from the literature (Matthes 1997). Calculations are conducted as shown below; the example was calculated using the number from Table 14:

1. Normalize all elements of the furnace lining to  $\text{Al}_2\text{O}_3$ :

$$F_i = \left( \frac{E_i(R)}{E_a(R)} \right) \quad (8)$$

$$\text{for example } F_{\text{CaO}} = \left( \frac{\text{CaO}(\text{lining})}{\text{Al}_2\text{O}_3(\text{lining})} \right) = \left( \frac{10}{20} \right) = 0.5 \text{ or } \quad (9a)$$

$$F_{\text{SiO}_2} = \left( \frac{\text{SiO}_2(\text{lining})}{\text{Al}_2\text{O}_3(\text{lining})} \right) = \left( \frac{70}{20} \right) = 3.5 \quad (9b)$$

2. Set  $\text{Al}_2\text{O}_3$  in the slag to zero

$$(E_a(S) = 0) \quad (10)$$

3. Remove adequate amounts of all elements from the slag according to the factor calculated in step 1:

$$E_i \text{ rest}(S) = E_i \text{ bulk}(S) - (E_a \text{ bulk}(S) \times F_i) \quad (11)$$

In our example,

$$\begin{aligned} \text{CaO rest}(S) &= \text{CaO bulk}(S) - (\text{Al}_2\text{O}_3(S) \times F_{\text{CaO}}) \\ &= 7 - (5 \times 0.5) = 7 - 2.5 = 4.5 \text{ or} \end{aligned} \quad (12a)$$

$$\begin{aligned} \text{SiO}_2 \text{ rest}(S) &= \text{SiO}_2 \text{ bulk}(S) - (\text{Al}_2\text{O}_3(S) \times F_{\text{SiO}_2}) \\ &= 38 - (5 \times 3.5) = 38 - 17.5 = 20.5 \end{aligned} \quad (12b)$$

**Table 14** Slag and furnace lining composition for calculation example (arbitrary numbers)

Chemical compound ( $E_i$ )	Slag ( $S$ ; fraction in wt.%)	Furnace lining ( $R$ ; fraction in wt.%)
FeO	50	0
Al <sub>2</sub> O <sub>3</sub>	5	20
CaO	7	10
SiO <sub>2</sub>	38	70

We see that the amount of Al<sub>2</sub>O<sub>3</sub> (5%)+SiO<sub>2</sub> (17.5%)+CaO (3.5%) removed from the slag yields a fraction of furnace lining in the slag of 26%. If  $E_a$  is present in more than one reactant (e.g., the charcoal ash may contain small amounts of Al or the lining may contain K), the order in which the reactants are removed from the slag is crucial. In any case the reactant with the smaller  $F_i$  should be removed first.

#### Attempt of a mass balance

The following calculations are conducted according to the procedure introduced above (Eq. 8–12). Due to the fact that the ash is the only component introducing considerable amounts of K<sub>2</sub>O to the slag, the ash analysis was K<sub>2</sub>O-normalized and all K<sub>2</sub>O as well as other elements were removed from the slag equivalently to the element/K<sub>2</sub>O ratio ( $F_{K_2O}$ ) in the ash.

It was not possible to determine the composition of the furnace lining because there are no archaeological finds of furnace material known from the area of Wiesloch. Therefore, the composition of the furnace lining had to be estimated. It was substituted by the analysis of a tenth century firing aid (which is a ceramic wedge, used in kilns to prevent the workpieces from sintering together) from Wiesloch. The firing aid was chosen as a substitute because the origin of the material (clay from the upper Pechelbronner Schichten), as well as its age (tenth century), is known (Hildebrandt 2001). The material was grogged with quartz sand, so the refractory qualities are present as well.

Aluminum was removed from the slag analysis using the Al-normalized firing aid analysis. The remaining elements were removed by transforming them to minerals: CO<sub>2</sub> was added to MgO+CaO to form dolomite, using the amount of MgO in the slag as restriction. The remaining CaO was removed by addition of CO<sub>2</sub> to form calcite. SiO<sub>2</sub> was removed as quartz; FeO, MnO, and TiO<sub>2</sub> were combined in an iron oxide flux. Unfortunately, the form of the iron flux is unknown (hematite, goethite,...), so the flux was calculated as FeO. Remaining BaO was transformed to barite by adding SO<sub>2</sub>.

Afterward, all components were recalculated as weight percent to obtain the ratio of iron flux, quartz flux, carbonate flux, barite flux, furnace lining, and charcoal ash.

The calculations yielded the following ranges

Furnace lining	29–52%	Mean 37%
Quartz flux	0–17%	Mean 3%
Carbonate flux (dolomite+calcite)	0–23%	Mean 10%
Iron flux (calculated as FeO)	20–46%	Mean 35%
Barite flux	0–17%	Mean 3%
Ash	9–17%	Mean 11%

The amount of ash is equivalent to 4.5–8.3 kg charcoal per kilogram slag, assuming an ash content of the charcoal of 2 wt.%. Unfortunately, the calculation of the fraction of furnace lining taken up by the slag yields some problems:

The calculation does not allow to distinguish between furnace lining and clay flux, which might be added to the charge to protect the furnace lining. So the amount predicted by the model might be a mixture of furnace

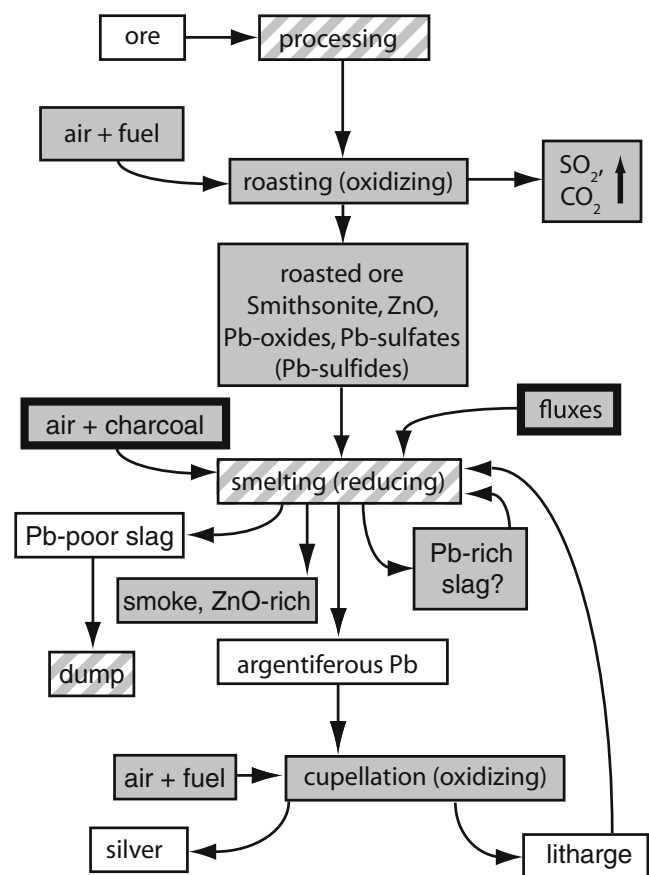


**Fig. 16** Flow scheme of all steps of silver production (modified after Bachmann 1993a). White boxes, archaeological findings and samples from Wiesloch (analysed); dashed boxes, proven by archeological excavation (Hildebrandt 1998); gray boxes, unknown factors

lining and clay flux. Another problem is the type of iron flux. There are manifold possibilities which material could have been used: natural materials like hematite, goethite, or Fe-hydroxides. Also anthropogenic materials like forging scales or smithing slags might have been used.

It is not possible to calculate a ratio of fluxes and ores. There is no element in the charge which occurs only in the ore and partitions completely to the silicate part of the slag during smelting. So including the ores to the calculations introduced in “Process Reconstruction” is not possible. The only way to solve this problem could be the calculation of the amount of energy gained by the combustion of a certain amount of charcoal, subtract the energy needed to form the slag, and keep it fluid and using the rest energy to reduce a certain amount of ore. However, these calculations contain too many assumptions to yield results of a useful precision.

The results show a high amount of furnace lining in the slag, pointing to a long smelting process in which much of the furnace lining was dissolved by the slag. This agrees well with what is known from the literature that a furnace cycle in a shaft furnace is longer compared to a bloomery furnace cycle. The mass balance for comparison with the bloomery process was published by Kronz and Keesmann (2003) and yields the following values:

$$92 \text{ wt.}\% \text{ ore} + 1 \text{ wt.}\% \text{ ash} + 7 \text{ wt.}\% \text{ furnace lining} \\ \rightarrow 55 \text{ wt.}\% \text{ iron} + 45 \text{ wt.}\% \text{ slag} \quad (13)$$

Although the model contains some uncertainties, the difference between our calculations and those of Kronz and Keesmann (2003) are significant and show a difference between slags from a bloomery process and those from a shaft furnace.

## Conclusions

This study provides a detailed database of phases, their composition and of the bulk composition of high-medieval lead–silver smelting slags. The results, especially the low-Pb content, indicate a sophisticated smelting technology, which resulted in the formation of a low viscosity slag with a surprisingly low liquidus temperature. This database can be used to calculate mass balances of the smelting process and thus a process reconstruction. It could be the background for an estimation of time and effort that needs to be conducted to keep a smelting site of the size of Wiesloch in good working condition. It is also possible to discriminate between short processes (bloomery) slags and those from longer lasting processes (non-ferrous metal slags). This is useful to gain information on slags with an incomplete context, or which are not in their original context any more.

During high-medieval times, it was highly likely that a mixture of argentiferous galmei and galena was smelted to produce lead and silver in Wiesloch. Unfortunately, we do not learn very much on the specific differences between “common” lead–silver smelting and the process conducted in Wiesloch. Further work is required on this type of ore smelting to gain knowledge on these differences. As long as there is no further evidence on a highly specialized smelting process, we have to assume an “adapted” process based on the common lead smelting process (Fig. 16). The process was a long-term process (compared to bloomery process), and it was run in shaft furnaces of unknown size using predominantly oak charcoal as fuel. The charges were composed of mixtures of ores and fluxes (iron oxide flux, carbonate flux, quartz flux, and barite flux) of varying composition. The process was conducted at  $\sim 1,100\text{--}1,200^\circ\text{C}$ , creating a low viscosity slag ( $\sim 0.5\text{--}20 \text{ Pa s}$ ) with a liquidus temperature of  $\sim 950\text{--}1,100^\circ\text{C}$ .

For the first time, we report a smelting process in which argentiferous galmei was added to the charge in significant amounts as a silver ore. The efficiency and the conditions of this process are unknown yet and will have to be investigated in laboratory and further smelting experiments.

**Acknowledgments** We are grateful to Michael Schneider, from the dendrochronological laboratory Hemmenhofen, who did the wood species determination on the charcoal, as well as Dr. Kromer, who did the sample preparation for the AMS. Thanks to the municipality of Wiesloch for the permission to do the excavation on public ground. Katharina Pfaff, Sebastian Staude and Nadja Huber are thanked for their insightful discussion and comments. Financial support was granted by the post-graduate ‘Promotionsverbund Wiesloch’ at the Universität Tübingen. We are very grateful to two anonymous reviewers, whose critical and constructive comments and discussion improved this work significantly.

## References

- Armstrong JT (1991) Quantitative elemental analysis of individual microparticles with electron beam instruments. In: Heinrich KFJ, Newbury DE (eds) Electron probe quantification. Plenum Press, New York, pp 261–315
- Bachmann H-G (1982) The identification of slags from archaeological sites. Institute of Archaeologie, University of London, London, Occasional publications 6
- Bachmann H-G (1993a) Vom Erz zum Metall (Kupfer, Silber, Eisen). Die chemischen Prozesse im Schaubild. Archäologie in Deutschland Sonderheft: Alter Bergbau in Deutschland, pp. 35–40
- Bachmann H-G (1993b) Zur Frühen Blei- und Silbergewinnung in Europa. Montanarchäologie in Europa - Freiburger Forschungen zum 1. Jahrtausend in Südwestdeutschland. H. Steuer and U Zimmermann 4:29–36
- Bachmann H-G, Lutz C, Thiemann U (1989) Schlackenviskositäten. Der Anschnitt Beiheft (Archäometallurgie der alten Welt) 7:137–140
- Battle TP, Hager JP (1990) Viscosities and activities in lead-smelting slags. Metall Mater Trans B 21 B:501–510

- Bauermeister J (2005) Archäometallurgische Untersuchungen von eisenschlacken aus dem Holtland/Kreis Leer. Göttingen, Diploma, Georg-August-Universität Göttingen
- Bauermeister J, Kronz A (2006) Phosphorreiche Erze: Ein Problem für die frühe Eisenverhüttung? Kaiserzeitliche Eisenverhüttung im Kreis Leer. Archäometrie und Denkmalpflege – Kurzberichte. O. Hahn and H. Stege. Stuttgart
- Craddock PT, Freestone IC, Gale NH, Meeks ND, Rothenberg B, Tite MS (1985) The investigation of a small heap of silver smelting debris from Rio Tinto, Huelva, Spain. Furnaces and Smelting Technology in Antiquity. Craddock PT and Hughes MJ. London, The British Museum. Occas Pap 48:199–217
- Degterov SA, Pelton AD (1999) Thermodynamic modeling of lead distribution among matte, slag, and liquid copper. Metall Mater Trans B 30:1033–1044
- Droop GTR (1987) A general equation for estimating  $\text{Fe}^{3+}$  concentrations in ferromagnesian silicates and oxides from microprobe analyses, using stoichiometric criteria. Mineralog Mag 51:431–435
- Eggers T (1999) Geochemische und phasenanalytische Untersuchungen an Schlacken aus dem SW-Harz. Institut für Geologie und Dynamik der Lithosphäre. Diploma Göttingen, Georg-August-Universität Göttingen
- Endell K, Müllensiefen W, Wagemann K (1932) Über die Viskositäten von Mansfelder Kupferhochofenschlacken in Abhängigkeit von Temperatur, chemischer Zusammensetzung und Krystallisation. Met Erz 29:368–375
- Ercker L (1580) Beschreibung aller fümemisten Mineralischen Ertzt vnnd Berckwercksarten. Frankfurt am Main, Johann Feyeraubend. digitized original, <http://echo.mpiwg-berlin.mpg.de>
- Ericsson T, Filippidis A (1986) Cation ordering in the limited solid solution  $\text{Fe}_2\text{SiO}_4\text{--Zn}_2\text{SiO}_4$ . Am Mineralog 71:1502–1509
- Ettler V, Legendre O, Bodénes F, Touray J-C (2001) Primary phases and natural Weathering of old lead–zinc pyrometallurgical slag from Příbram, Czech Republic. Can Mineralog 39:873–888
- Faber W (1936) Die Mineralien der Bleischlacken. Anwendung gesteinskundlicher Untersuchungsmethoden auf Schlacken. Chem Erde 10(1):67–115
- Goldenberg G, Otto J, Steuer H (1996) Archäologische Untersuchungen zum Metallhüttenwesen im Schwarzwald. Jan Thorbecke, Sigmaringen
- Hauptmann A, Pernicka E, Wagner GA (1988) Untersuchungen zur Prozesstechnik und zum Alter der frühen Blei-Silbergewinnung auf Thasos. Der Anschnitt Beiheft 6:88–112
- Hauptmann A, Rehren T, Schmitt-Strecker S (2003) Early Bronze Age copper metallurgy at Shahr-i Sokhta (Iran), reconsidered (Schlacken+Speiss). Der Anschnitt Beiheft (Mensch und Bergbau) 16:197–213
- Hildebrandt LH (1997) Schwermetallbelastungen durch den historischen Bergbau im Raum Wiesloch. L. f. U. Baden-Württemberg. Wiesloch
- Hildebrandt LH (1998) Schwermetallbelastungen durch historischen Bergbau im Raum Wiesloch. Dissertation Heidelberg, Ruprecht-Karls-Universität
- Hildebrandt LH (2001) Mittelalterarchäologie in Wiesloch, Teil1: Die Wüstung Westenweiler am Hoschket (7.-10- Jahrhundert). Wiesloch - Beiträge Zur Geschichte 2:49–67
- Hildebrandt LH (2004) 2000 Jahre Blei-Zink-Silber-Bergbau in Wiesloch bei Heidelberg – Eine Übersicht. Zeitschrift zur Geschichte des Berg- und Hüttenwesens 10(2):4–26
- Hildebrandt LH (2005) "Ferrum, plumbum et argentum: Spuren des römischen Bergbaus." Begleitband zu Landesausstellung "Imperium romanum" Stuttgart: 399–402
- Ilisch L, Lorenz S, Stern WB, Steuer H (2004) Dirham und Rappenpfennig. Mittelalterliche Münzprägung in Bergbauregionen. Zeitschrift für Archäologie des Mittelalters Beiheft 17
- Jianping L, Kornprobst J, Laporte D (1999) Subsolidus phase relations in the system  $\text{MgO--ZnO--SiO}_2$  at high pressure. Chin Sci Bull 44 (12):1146–1149
- Kappes BA (2000) Mobilisierbarkeit von Schwermetallen und Arsen durch Saure Grubenwässer in Bergbaualtlasten der Ag–Pb–Zn-Lagerstätte Wiesloch. Karlsruher Geochemische Hefte 13:1–206
- Kassianidou V (1998) Was silver actually recovered from speiss in antiquity? Der Anschnitt Beiheft 8 Metallurgia Antiqua
- Kongoli F, Yazawa A (2001) Liquidus surface of  $\text{FeO--Fe}_2\text{O}_3\text{--SiO}_2\text{--CaO}$  slag containing  $\text{Al}_2\text{O}_3$ ,  $\text{MgO}$ , and  $\text{Cu}_2\text{O}$  at intermediate oxygen partial pressures. Metall Mater Trans B 32(4):583–592
- Kronz A (1994) Pauschalchemische Analyse mittels Elektronenstrahlmikroskopie am Beispiel eisenreicher Schmelzpräparate. Eur J Mineral 6(1, Beiheft)
- Kronz A (1997) Phasenbeziehungen und Kristallisationsmechanismen in fayalitischen Schmelzsystemen - Untersuchungen an Eisen- und Buntmetallenschlacken. Fakultät für Geowissenschaften. Dissertation Mainz, Johannes Gutenberg Universität
- Kronz A (2005) Erzbergbau, Buntmetallmineralisationen und Silber-Metallurgie im Bereich der mittleren Mosel. Zeitschrift zur Geschichte des Berg- und Hüttenwesens (Fischbacher Hefte) 11(1)
- Kronz A, Eggers T (2001) Archäometallurgische Untersuchungen eisenzeitlicher Funde aus dem Hügelgräberfeld Hillesheim. Trier Z 64:69–109
- Kronz A, Keesmann I (2003) Fayalitische Schmelzen und die Effektivität des metallurgischen Verfahrens. Abbau und Verhüttung von Eisenerzen im Vorland der mittleren Schwäbischen Alb, Forschungen und Berichte zur Vor- und Frühgeschichte in Baden-Württemberg. 259–274
- Kronz A, Zolgamian Z, Maier P, Keesmann I (1992) "Rhönit  $\text{Ca}_4(\text{Fe}^{2+}, \text{Fe}^{3+}, \text{Mn}, \text{Al}, \text{Ti})_{12}[(\text{Al}, \text{Si})_{12}\text{O}_{40}]$  in historischen Schlacken." Berichte der Deutschen Mineralogischen Gesellschaft, Beiheft z. European Journal of Mineralogy 4(1)
- Leeman WP, Scheidegger KF (1977) Olivine/liquid distribution coefficient and a test for crystal-liquid equilibrium. Earth Planet Sci Lett 35:247–257
- Matthes WE (1997) Keramische Glasuren: Ein Handbuch mit 1100 Rezepten. Augsburg
- Mone F (1859) Römisches Bergwerk zu Wiesloch. Zeitschrift zur Geschichte des Oberrheingrabens 10:389
- Mukhopadhyay DK, Lindsley DD (1983) Phase relations in the join  $(\text{CaFeSiO}_4)\text{--fayalite}$  ( $\text{Fe}_2\text{SiO}_4$ ). Am Mineralog 68:1089–1094
- Muszer A (2006) Petrographical and mineralogical characteristics of the metallurgical slag from the Dörschl furnace (Glogów Foundry, Poland). Physicochemical Problems of Mineral Processing 40:89–98
- Nikolic S, Hayes PC, Yak E (2008a) Phase equilibria in ferrous calcium silicate slags: part I. Intermediate oxygen partial pressures in the temperature range 1200°C to 1350°C. Metall Mater Trans B 39(B)
- Nikolic S, Henao H, Hayes PC, Yak E (2008b) Phase equilibria in ferrous calcium silicate slags: part II. Evaluation of experimental data and computer thermodynamic models. Metall Mater Trans B 39:189–199
- Okamoto H (1991) The Fe–As system. J Phase Equilibria 12(4):457–461
- Osborn EF, Muan A (1960) Phase equilibrium diagrams of oxide systems. Ceramic foundation, Columbus
- Pawlek F (1983) Metallhüttenkunde. DeGruyter, Berlin
- Pernicka E (1981) Archäometallurgische Untersuchungen zur antiken Silbergewinnung in Laurion 1. Chemische Analyse griechischer Blei-Silber-Erze. Erzmetall 34(8)
- Pernicka E (1983) Archäometallurgische Untersuchungen zur antiken Silbergewinnung in Laurion 3. Das Verhalten einiger Spurenelemente beim Abtreiben des Bleis. Erzmetall 36(12)

- Pernicka E, Lutz C, Bachmann H-G, Wagner GA, Elitzsch C, Klein E (1985) Alte Blei-Silber Verhüttung auf Sifnos. Der Anschnitt Beiheft (Silber Blei und Gold auf Sifnos) 3:185–199
- Pfaff K, Hildebrandt LH, Leach DL, Jacob DE, Markl G (2010): Formation of the Mississippi Valley-Type Zn-Pb-Ag deposit in the extensional setting of the Upper Rhinegraben in the Wiesloch area, SW Germany. *Mineralium Deposita*. doi:10.1007/s00126-010-0296-5.
- Reimer PJ, Baille MGL, Bard E, Bayliss A, Beck JW, Bertrand CJH, Blackwell PG, Buck CE, Burr GS, Cutler KB, Damon PE, Edwards RL, Fairbanks RG, Friedrich M, Guilderson TP, Hogg AG, Hughen KA, Kromer B, McCorman G, Manning S, Ramsey CB, Reimer RW, Remmele S, Southon JR, Stuiver M, Talamo S, Taylor FW, Pflücht JVD, Weyhenmeyer CE (2004) INTCAL 04 terrestrial radiocarbon age calibration, 0–26 Kyr BP. *Radiocarbon* 46(3):1029–1058
- Sarver JF, Hummel FA (1962) Solid solubility and eutectic temperature in the system  $Zn_2SiO_4$ – $Mg_2SiO_4$ . *J Am Ceram Soc* 45(6): 304
- Schlesinger ME, Lynch DC (1986) PbO solubility in lead-blast furnace slags. *Metall Mater Trans B* 17(4):817–827
- Seeliger E (1963) Die Paragenese der Pb-Zn-Erzlagerstätte am Gänsberg bei Wiesloch (Baden) und ihre genetische Beziehung zu den Gängen im Odenwaldkristallin, zu Alt Wiesloch und der Vererzung der Trias des Kraichgaues. *Jahreshefte des geologischen Landesamtes Baden-Württemberg* 6:239–299
- Skog G (2007) The single stage AMS machine at Lund University: status report. *Nucl Instrum Meth Phys Res B* 259:1–6
- Smuts J (1992) Formation and morphology of iron silicate ‘iscorite’. *Ironmak Steelmak* 19(2):111–119
- Smuts J, Steyn JGD, Boeyens JCA (1968) The crystal structure of an iron silicate, iscorite. *Acta Crystallogr B* 27(7):1251–1255
- Thornton CP, Rehren T, Pigott VC (2009) The production of speiss (iron arsenide) during the Early Bronze Age in Iran. *J Archaeol Sci* 36:308–316
- Van Aken PA, Mieke G, Woddlund AB, Angel RJ (2005) Crystal structure and cation distribution in  $Fe_7SiO_{10}$  (“Iscorite”). *Eur J Mineral* 15(5):723–731